OROGRAPHIC GRAVITY-WAVE DRAG: ITS PARAMETRIZATION AND INFLUENCE IN GENERAL CIRCULATION AND NUMERICAL WEATHER PREDICTION MODELS

M.J. Miller and T.N. Palmer
European Centre for Medium-Range Weather Forecasts
Reading, U.K.

1. INTRODUCTION

Until quite recently, the design of a numerical weather prediction (NWP) model was quite different to that of a general circulation model (GCM). Because NWP models were only integrated for a few days at a time, great emphasis was placed on optimising the adiabatic formulation and achieving as high a resolution as possible. In GCMs, on the other hand, a compromise between model resolution and sophistication of physical parametrizations was necessary, given available computer resources. As a result, systematic biases in medium or high resolution models could easily be overlooked, either because NWP models were not integrated long enough for the amplitude of these biases to be apparent, or because GCMs were not of sufficiently high resolution.

Increased computer resources have blurred the distinction between the GCM and NWP model, and have highlighted one such bias. In this paper we produce evidence, entirely from model integrations, that suggests that the bias is associated with the usual representation of orography in numerical models, and can be largely be alleviated by parametrizing directly the drag effect of sub-gridscale orography (on scales where buoyancy forces are important) and gravity wave excitation is efficient.

This evidence is discussed in Section 2 where other possible 'cures', such as enhanced surface roughness or enhanced large-scale orography, are considered. A specific parametrization, as currently used in the ECMWF model, is described in Section 3, and its effect on forecast skill and on 'climate' simulation is discussed in Sections 4 and 5 respectively.

2. GRAVITY-WAVE DRAG WITHOUT GRAVITY-WAVE DRAG

Palmer et al. (1986) and Shutts (1986) gave a synopsis of the observational evidence for gravity-wave drag (GWD), including results from aircraft studies, microbarograph measurements of pressure drag, and residual calculations from large-scale analyses; also some of the papers in this seminar deal explicitly with results from observational studies. Therefore we have decided to take a somewhat different approach here in motivating use of the gravity-wave parametrization. Specifically, we shall take an 'inverse' approach and try to discover from a series of modelling experiments the sort of mechanism that must be invoked in order to correct the observed bias (see below) in medium and high resolution GCMs. We shall try to argue that the parametrization so obtained contains some very specific requirements that appear to be consistent with the theory of, and observational evidence for, orographic GWD. This approach to the problem motivated the title to this section.

In the last few years, Manabe and Hahn (1981), and Pitcher et al. (1983) have described the climatology of two different general circulation models, both with truncation at R15. The models were integrated for several years of model time so that statistically significant estimates of climatological quantities could be obtained. Results for the northern hemisphere flow were impressive with, for example, a zonal mean flow of about the correct strength and a realistic time-mean surface pressure field. By contrast, however, the southern hemisphere flow was poorly simulated in both models. In particular the zonal mean flow was too weak and, at the surface, the sub-Antarctic trough was not deep enough.

A similar behaviour is found in the ECMWF T21 model (Von Storch et al., 1985) and for grid point models at similar resolution. To demonstrate the latter point, Figs 1a, 2a, and 3a show the surface pressure distribution and zonal mean wind cross-section from a 90-day wintertime integration of the Meteorological Office (UKMO) climate model with a regular latitude/longitude grid, which for this experiment has a spacing of 5 x 7.5 degrees. Observed climatological fields are shown in Figs 1d, 2d and 3d. The model was integrated in annual cycle mode using initial data from 6 December 1983. The weakness of the surface flow in the southern hemisphere is quite clear (compare Figs 1a and 1d).

These results, taken by themselves, suggest that if there is a systematic error to correct in GCMs, it is not associated with major deficiences in the northern hemisphere. The notion that the absence of a parametrization of orographic GWD is associated with such systematic errors seems, on the face of it, rather unlikely. In view of this, one can understand that the development of parametrizations of sub-gridscale orography was not considered to be a major priority until recently.

Why has the situation changed? Mainly because increased computing power has meant that GCMs can now be run at higher resolutions than R15 or T21. Naively one might imagine that enhancing the model resolution would improve its climatology. As it turns out, this is true for simulations of the southern hemisphere flow, but is certainly not true for the northern hemisphere flow. Figs 1b-c, 2b-c and 3b-c show 90-day mean surface pressure and 90-day mean zonal wind cross-sections from integrations of two different medium resolution models, the UKMO climate model with a regular 2.5 x 3.75 degrees grid, and the ECMWF spectral model with T42 truncation. As before, both models were

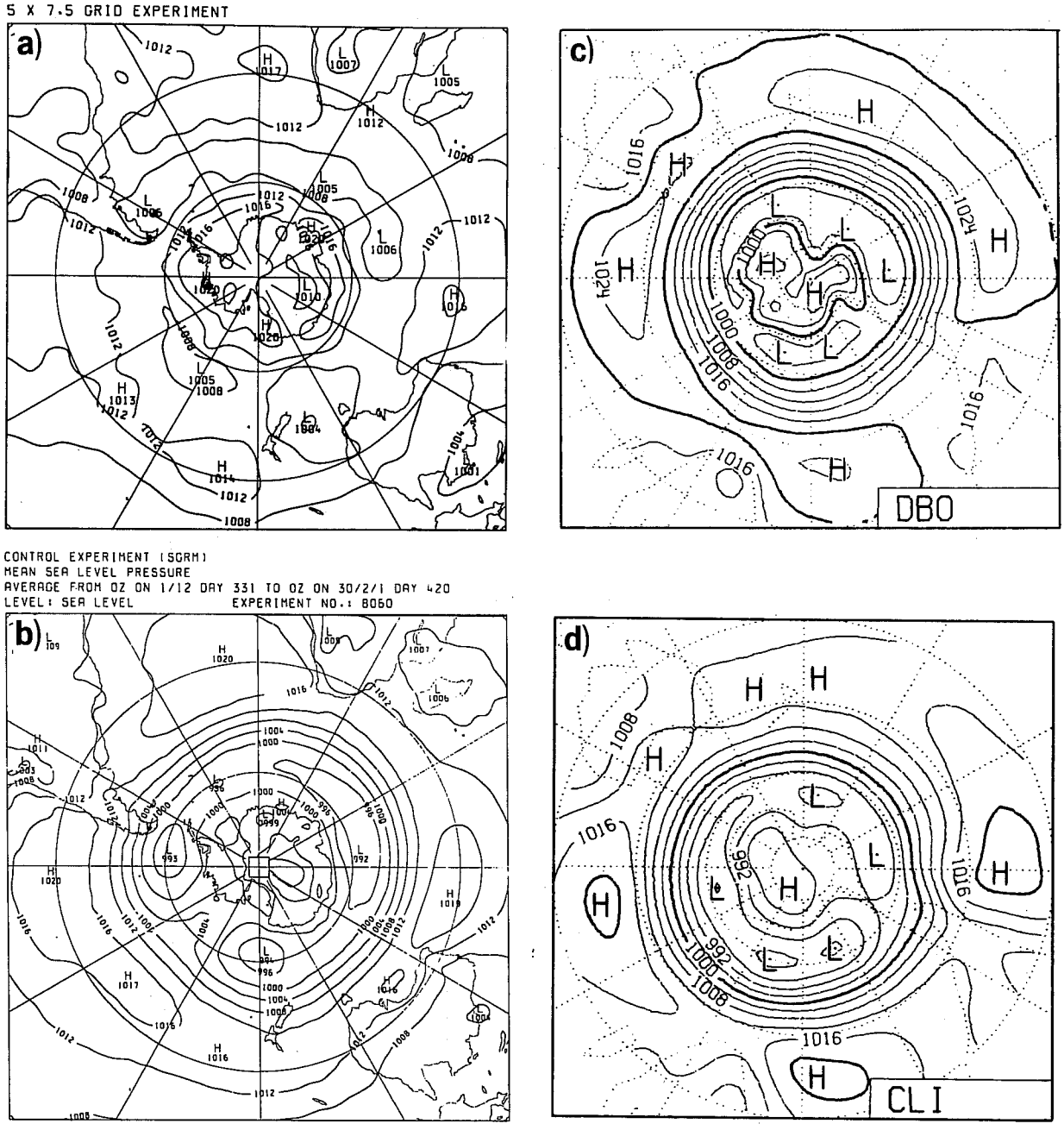

Fig. 1 Mean Southern Hemisphere surface pressure (mb) from 90-day Northern Hemisphere wintertime integrations (with mean orography) of
a) UKMO climate model with 5x7½° lat/long resolution
b) UKMO climate model with 2½x3¾° lat/long resolution
c) ECMWF model with T42 resolution
d) Observed climate

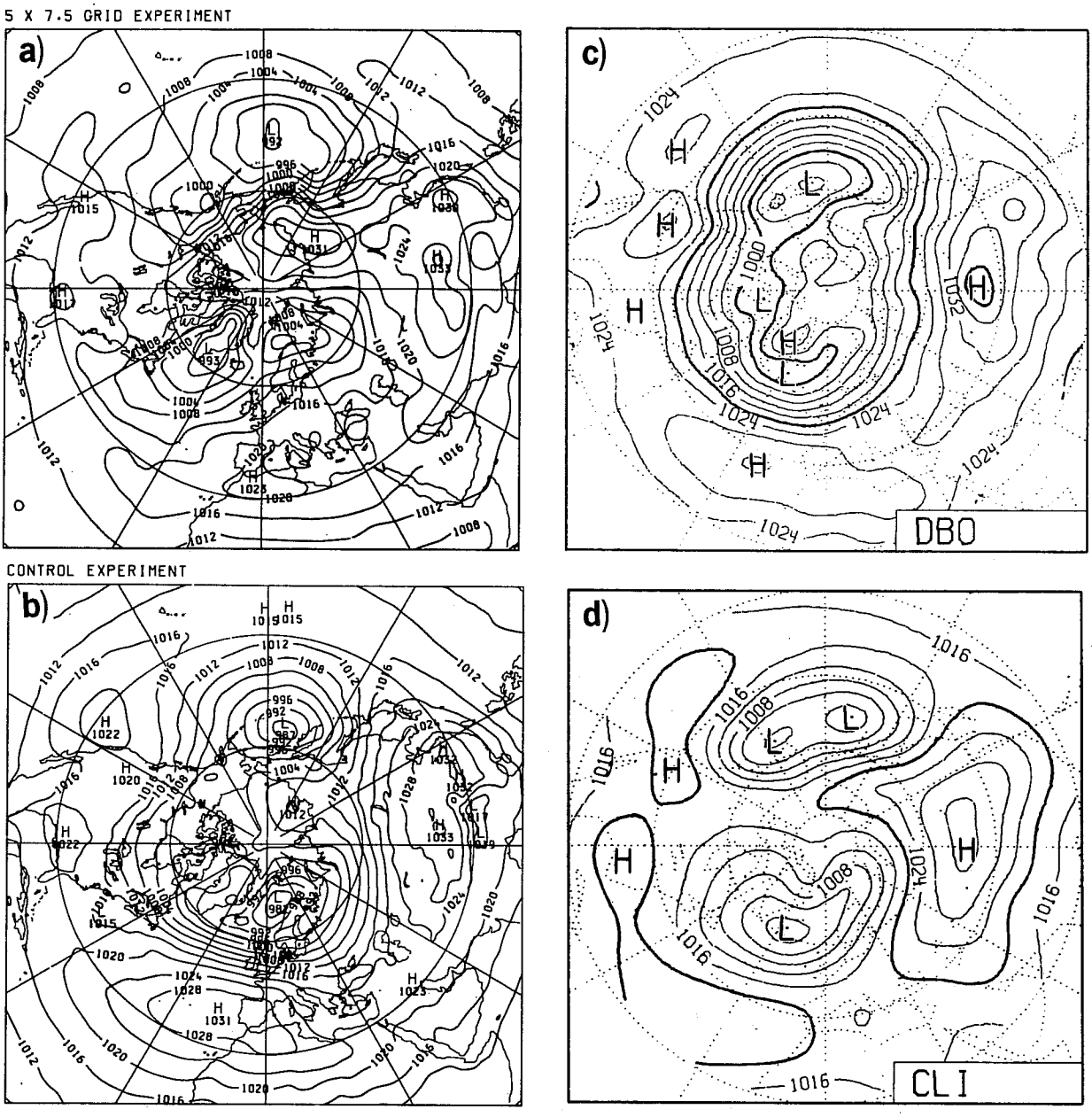

Fig. 2 As Fig. 1 but for Northern Hemisphere surface pressure (mb).

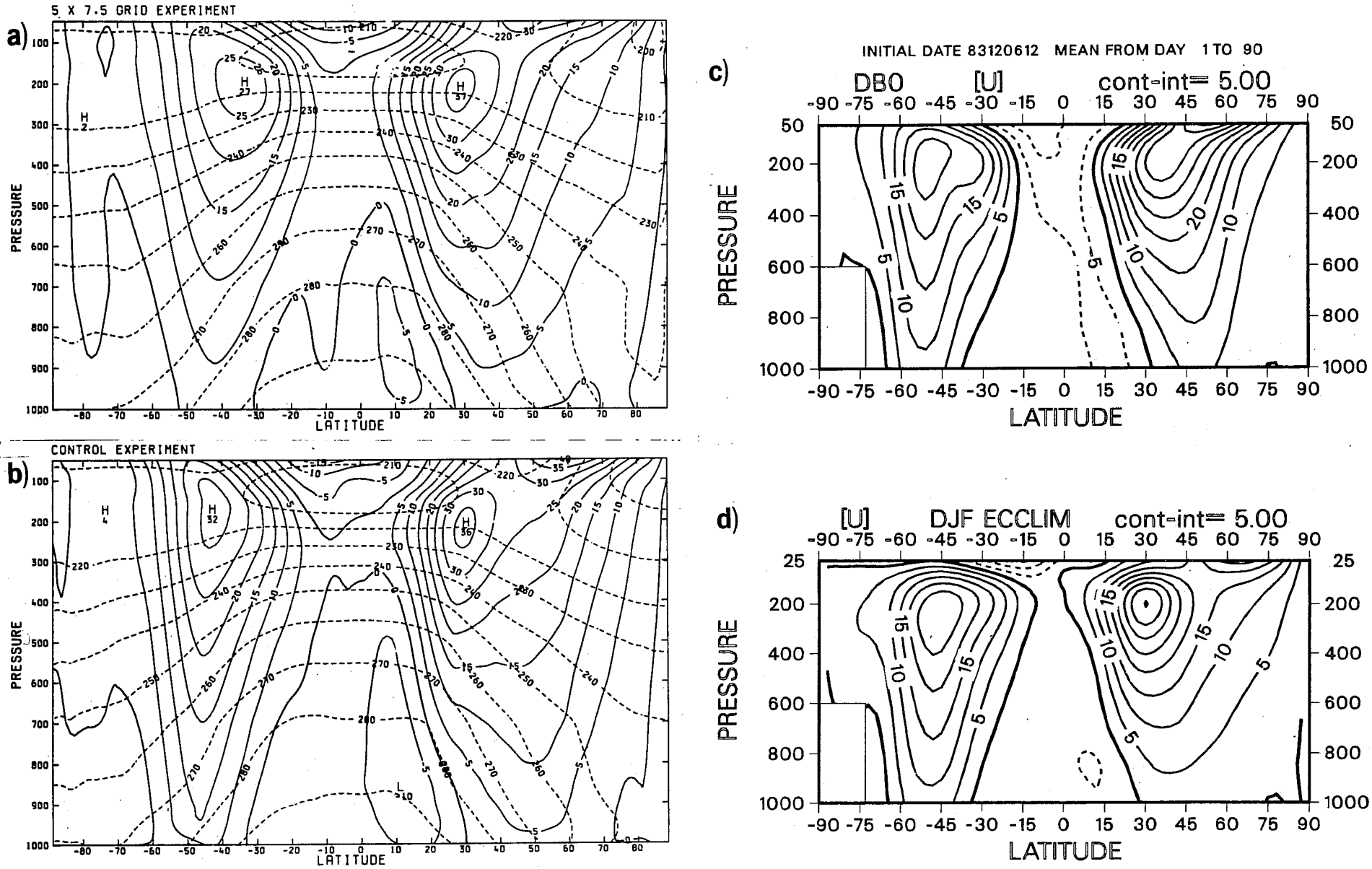

Fig. 3 As Fig. 1 but for zonal mean zonal wind cross sections (ms^{-1}).

integrated in annual cycle mode using initial data from 6 December 1983. The 90-day mean fields show that both models have simulated the strength of the southern hemisphere flow fairly well, and the depth of the sub-Antarctic trough is much improved compared with any of the low resolution models cited above. The northern hemispere flow has deteriorated, however. At the surface, the Icelandic and Aleutian Lows are too deep and generally ill-positioned. Across the continents the strong surface westerlies continue, largely unabated. The excessive zonal flow is manifest at all levels in the model. (M. L. Blackmon, personal communication, has reported similar behaviour when the NCAR Community Climate Model is integrated at R30 truncation.)

So increasing resolution alone has had the somewhat perverse effect of shifting the focus of attention, as far as systematic error is concerned, from the southern to the northern hemisphere. Clearly, before suggesting possible ways of alleviating this problem, we should try to understand why the flow is so sensitive to model resolution. In doing so, it is worth recalling some very basic ideas on the maintenance of the surface westerlies in the extratropics. As Jeffries (1933) pointed out, frictional coupling between the atmosphere and the ground would, by itself, destroy the extratropical surface westerlies in a matter of days. He then went on to to show that the mid-latitude cyclones play an essential role in providing a flux of westerly momentum from the tropics into mid-latitudes, balancing the flux of westerly momentum, due to friction, from the mid-latitude atmosphere to the ground.

More generally, one can describe the momentum budget in the extratropics in terms of a balance between frictional stress and large-scale mountain torque on the one hand, and convergence of the northward flux of westerly momentum on

the other. Fig 4 shows the eddy flux <u'v'> at 250mb, averaged over 90 days for the integrations of the UKMO climate model with 5 x 7.5 degree and 2.5 x 3.75 degree resolution. Also shown are observed values from one winter. It can be seen that the low resolution model underestimates <u'v'> by about a factor of two compared with the higher resolution model.

That momentum fluxes are generally underestimated in low resolution GCMs is further supported by results from Cubasch's (1981) study from ECMWF models of varying resolution. Fig 5 shows horizontal momentum fluxes for a 24-day mean, taken from the last 24 days of 50 day integrations of various resolution models at ECMWF. It can be seen that increasing horizontal resolution from T21 to T40 has a dramatic effect on <u'v'>. Interestingly, increasing vertical resolution appears also to have a modest impact.

These results are extremely important as they indicate that if low resolution models do simulate the northern hemisphere surface westerlies more or less correctly, they must do by compensating for inadequate horizontal momentum fluxes through insufficient frictional stress or mountain torque. Since the southern hemisphere flow is too weak in such models, one can immediately rule out the possibility of inadequate frictional stress over the oceans. Hence either the frictional stress over land or the resolved mountain torque must be too weak.

At this stage, it would be unreasonable to introduce a new physical parametrization, such as orographic GWD, without first examining whether adjustments to existing parametrization schemes can help alleviate the problem of these excessive westerlies. In view of the above conclusion, two possible modifications immediately come to mind. Firstly, frictional stress over land

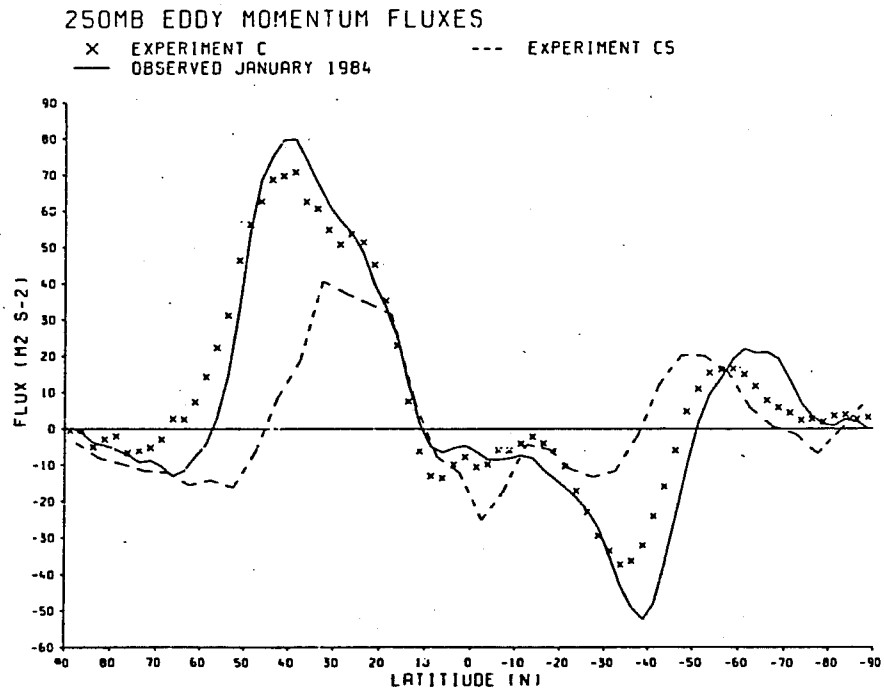

Fig. 4 250 mb horizontal momentum flux ($m^s s^{-2}$), averaged over 90 days, for UKMO model integrations (shown above) with $5 \times 7\frac{1}{2}$ (C5) and $2\frac{1}{2} \times 3\frac{3}{4}°$ (C) resolution. Observations for January 1984 are also shown.

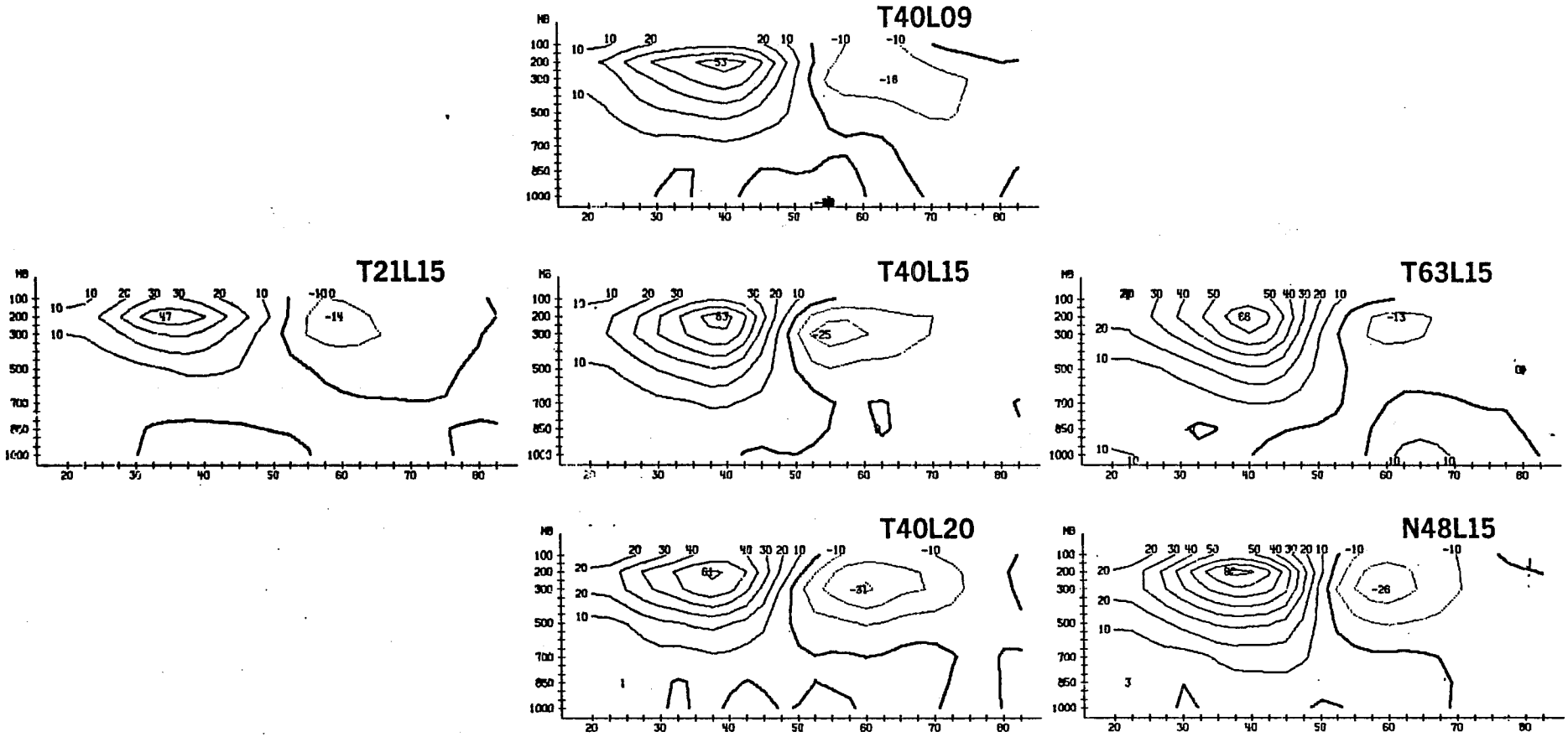

Fig. 5 Cross sections of 24-day mean horizontal momentum fluxes for ECMWF models with various resolutions.

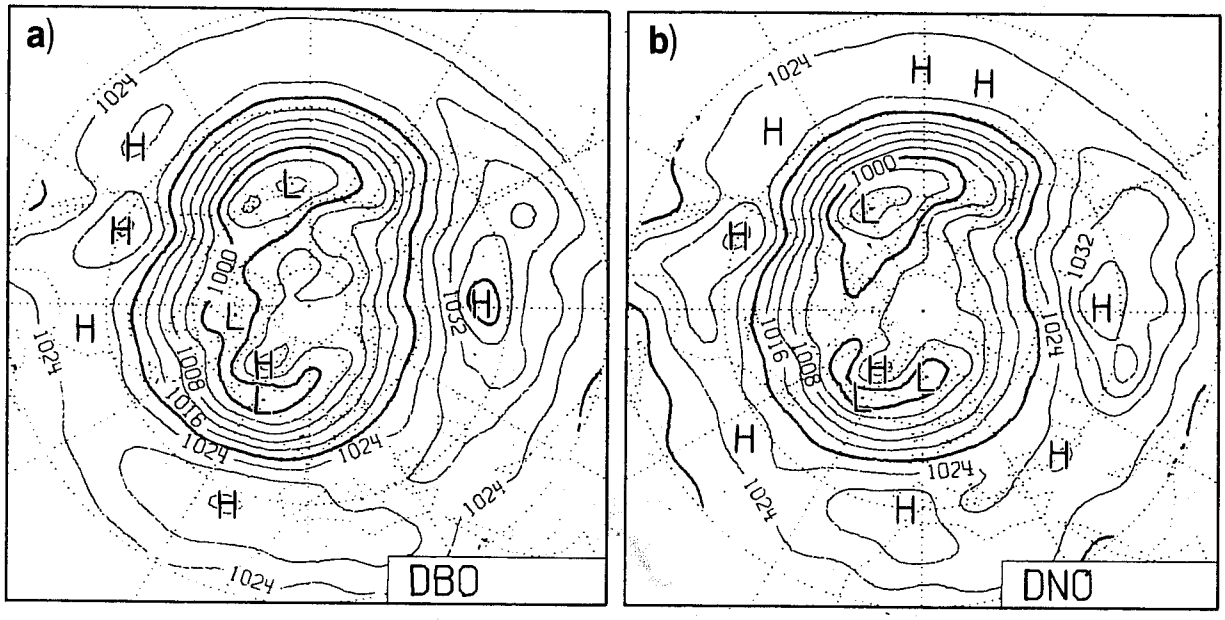

Fig. 6 Mean Northern Hemisphere surface pressure (mb) from 90-day wintertime integrations of the ECMWF T42 model with mean orography and
a) operational values for surface roughness lengths
b) doubled surface roughness length for momentum transfer.

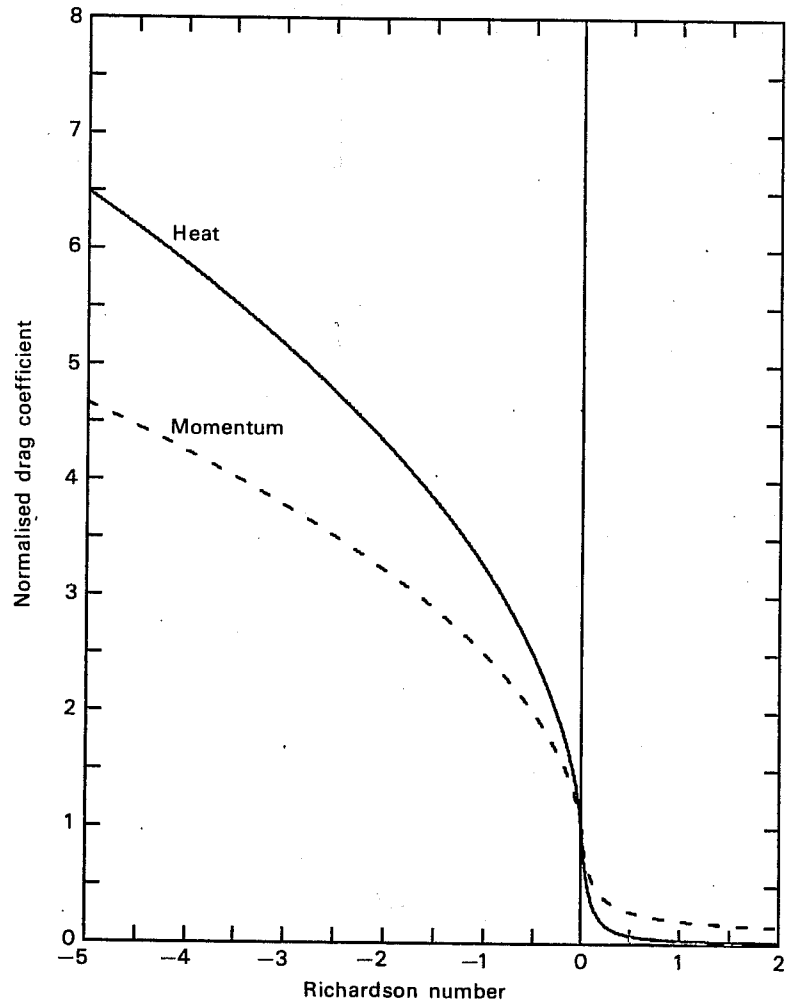

Fig. 7 Drag coefficients for heat and momentum as a function of Richardson number, in the ECMWF model.

could be increased by enhancing land surface roughness lengths. Maybe, one might argue, such an increase is justified as a means of including effects of sub-gridscale orography. Secondly, as Tibaldi (1987) has shown, the inclusion of the envelope orography parametrization (Wallace et al., 1983) will increase mountain torques.

In order to test whether such modifications have a beneficial effect on model climate, some further 90-day integrations have been run with the ECMWF T42 model and the UKMO 2.5 x 3.75 degree model, both from 6 December 1983. The experiments include firstly a doubling of the surface roughness length, and secondly inclusion of an envelope orography which consists of adding twice the observed standard devation of sub-gridscale orography (obtained from the U.S. Navy, dataset) to mean gridpoint values.

Results shown in Fig 6 indicate that the enhanced roughness lengths have little impact on the basic simulation of the large-scale flow. Perhaps, on reflection, one should not be suprised about this. Conventional boundary layer friction parametrizations attempt to describe the pressure drag associated with flow separation, and turbulent dissipation in the wake of small-scale roughness elements. Since stability will tend to suppress such flow separation and the subsequent vertical diffusion of momentum in the turbulent wake, one can expect the flow to be largely insensitive to roughness length under stable conditions. Fig 7, for example, shows the drag coefficient for momentum in terms of the Richardson number, Ri, for the ECMWF model. The coefficient is some ten times larger when Ri=-1 than when Ri=+1.

Envelope orography, on the other hand, clearly does have a substantial impact on the large-scale flow. The surface flow is weakened over the continents (Fig 8a) and the mean zonal mean wind cross-section shows generally reduced values in the mid-latitude northern hemisphere (Fig 9a). However, there are also undesirable features in the model climate. Fig 10a shows that the erroneous strong and persistent anticyclone over the Azores is associated with an intense ridge in the 200mb flow. The main jet is diverted to the north of the British Isles and the observed diffluence of the jet over western Europe is not simulated. Similarly, the 200mb flow over Alaska and Canada is too strong.

As will be shown for the ECMWF model below, the absence of adequate diffluent flow over the eastern oceans appears to be associated with the inability of the model to simulate realistic low-frequency variability (transitions from blocked to non-blocked flow, for example) in these regions. As many diagnostic studies appear to show (see Hoskins et al., 1986, and references therein) individual anomalous weather regimes (a block, for example) are maintained by the interaction between transient eddy activity associated with synoptic scale systems and the time mean flow. In common with theories of wave, mean-flow interaction between the zonal mean flow, and deviations therefrom, (Charney and Drazin, 1961), the efficacy with which such interaction takes place may depend on how dissipative the eddy field is. As we will show later, storm-track activity is insufficiently damped over the continents with mean orography, and the situation is barely improved with envelope orography. As a result, it is possible that errors in simulating the time-mean jet are ultimately related to the way in which cyclonic activity is damped over land.

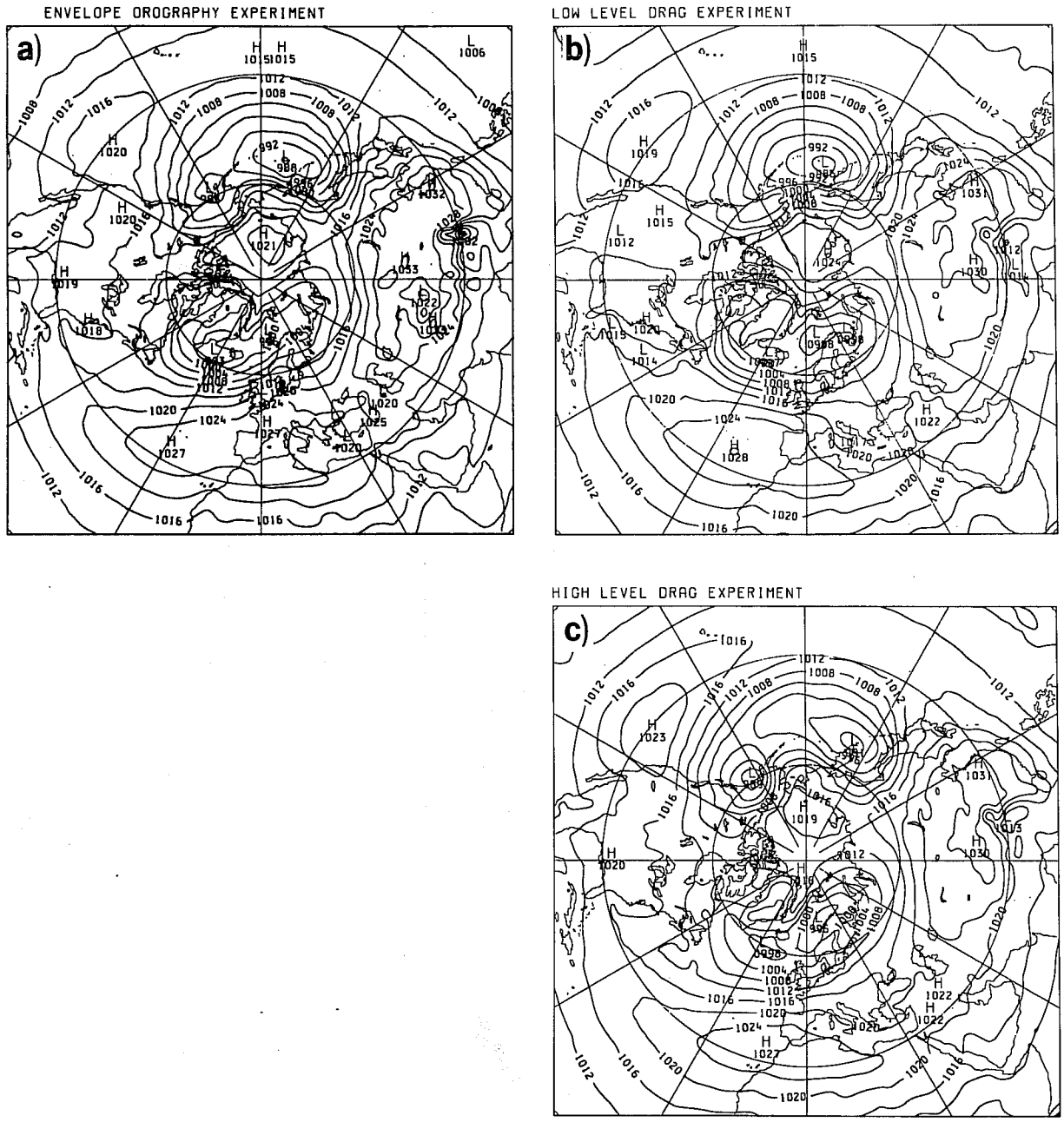

Fig. 8 Mean Northern Hemisphere surface pressure (mb) from 90-day wintertime integrations of the UKMO climate model with $2\frac{1}{2}$x$3\frac{3}{4}$° resolution and
a) 2σ envelope orography
b) low-level 'thermal' drag
c) high-level 'thermal' drag

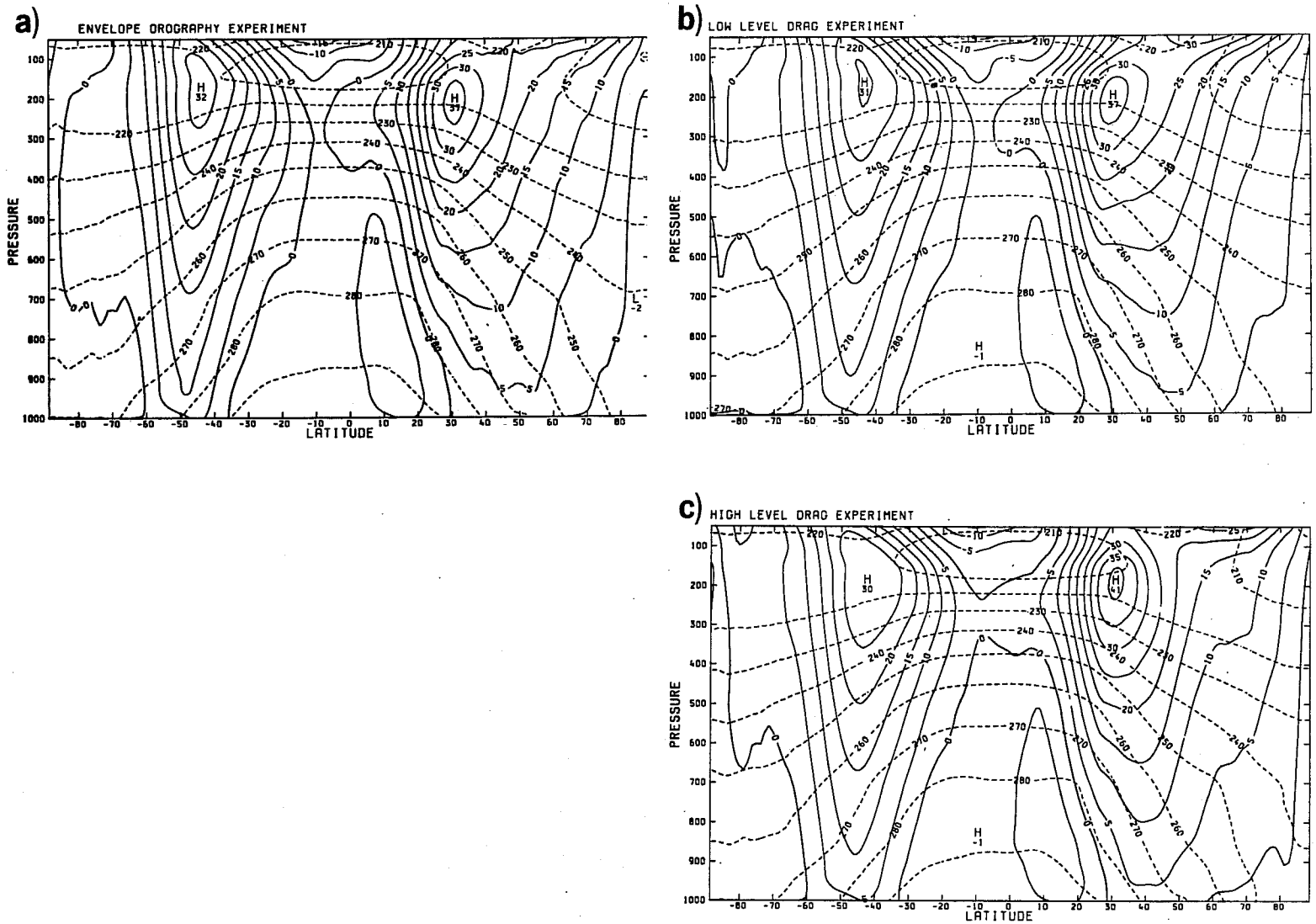

Fig. 9 As Fig. 8 but for zonal mean zonal wind cross section (ms^{-1}).

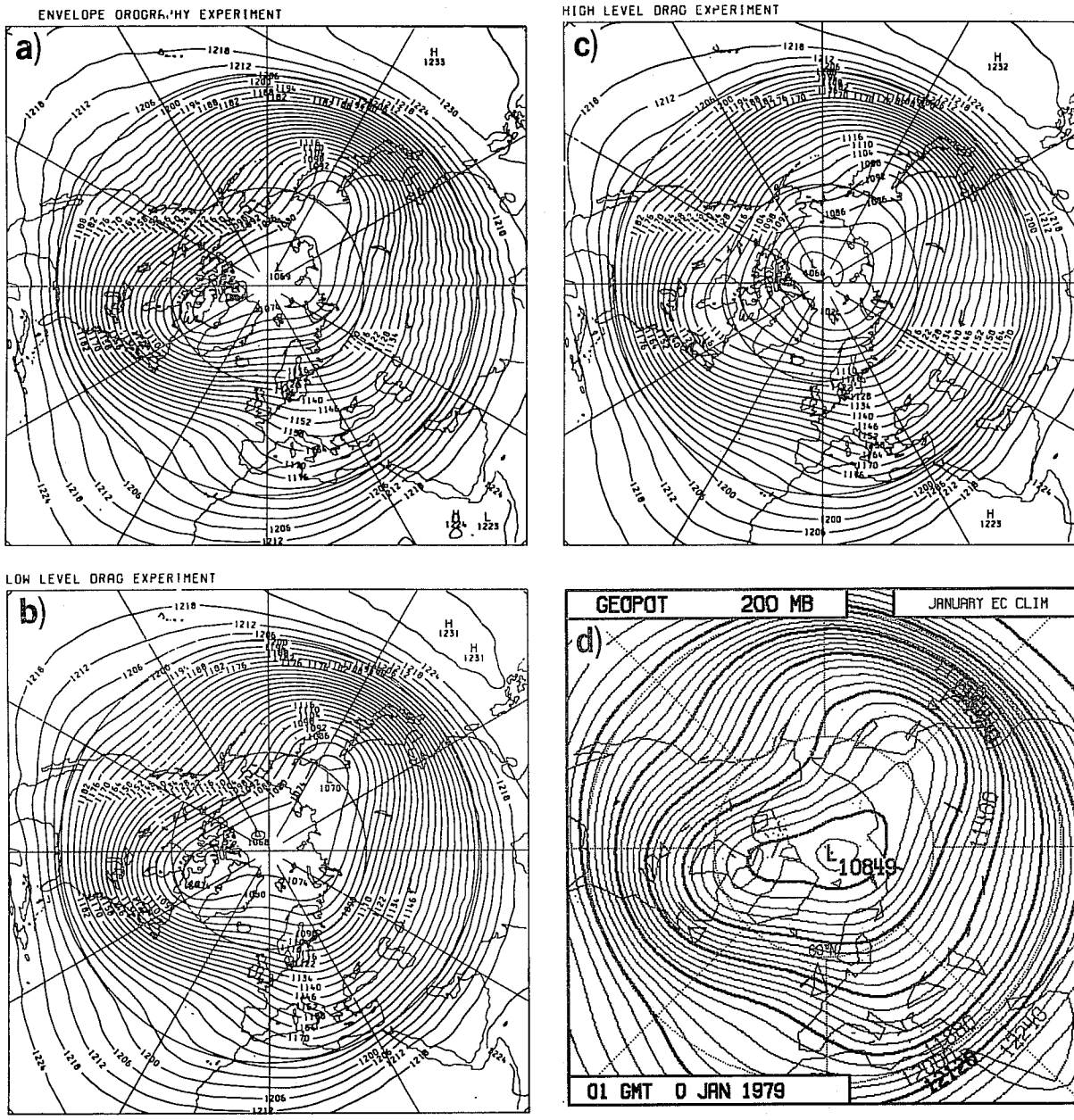

Fig. 10 As Fig. 8 but for 200 mb height (dam). (with d) observed climate.

Returning to the question of increasing the frictional coupling between land and atmosphere, it is not difficult to circumvent the ineffectiveness of the surface friction parametrization discussed above. If the horizontal dimension of a roughness element is much greater than U/N, where U is wind speed and N the buoyancy frequency, then simple dimensional arguments dictate that the pressure drag across the roughness element will depend on thermal, rather than inertial effects (the effect parametrized by boundary layer friction). Since U/N is of the order of 1 km, such elements will be representative of orography rather than, say, buildings or vegetation. Such a 'thermal' drag will depend on the stability of the flow, its wind speed, and the 'roughness' of the small-scale orographic features. A simple such parametrization of this effect would be to make the dependency linear, and represent the orographic roughness parameter by the sub-gridscale variance of orographic height (Var) which is available from the envelope orography calculation.

Consider, therefore, the effect of incorporating the surface stress

$$\tau = KU_s N_s (Var)$$

into the model formulation. For reasons discussed below, we take the value of the constant K to be equal to 2.5×10^{-5} m^{-1}.

In addition we must decide how this stress is distributed in the vertical. The following two experiments test the impact of the parametrization with two idealised profiles. In the first the surface stress is absorbed uniformly in the bottom three model layers, in the second it is absorbed uniformly in the top three model layers. Results are shown in Figs 8-10 for experiments with the UKMO. Unlike the experiment with doubled roughness length, this parametrization has a substantial impact. To first order one could argue that the surface pressure distribution (Fig 8b,c) does not depend strongly on

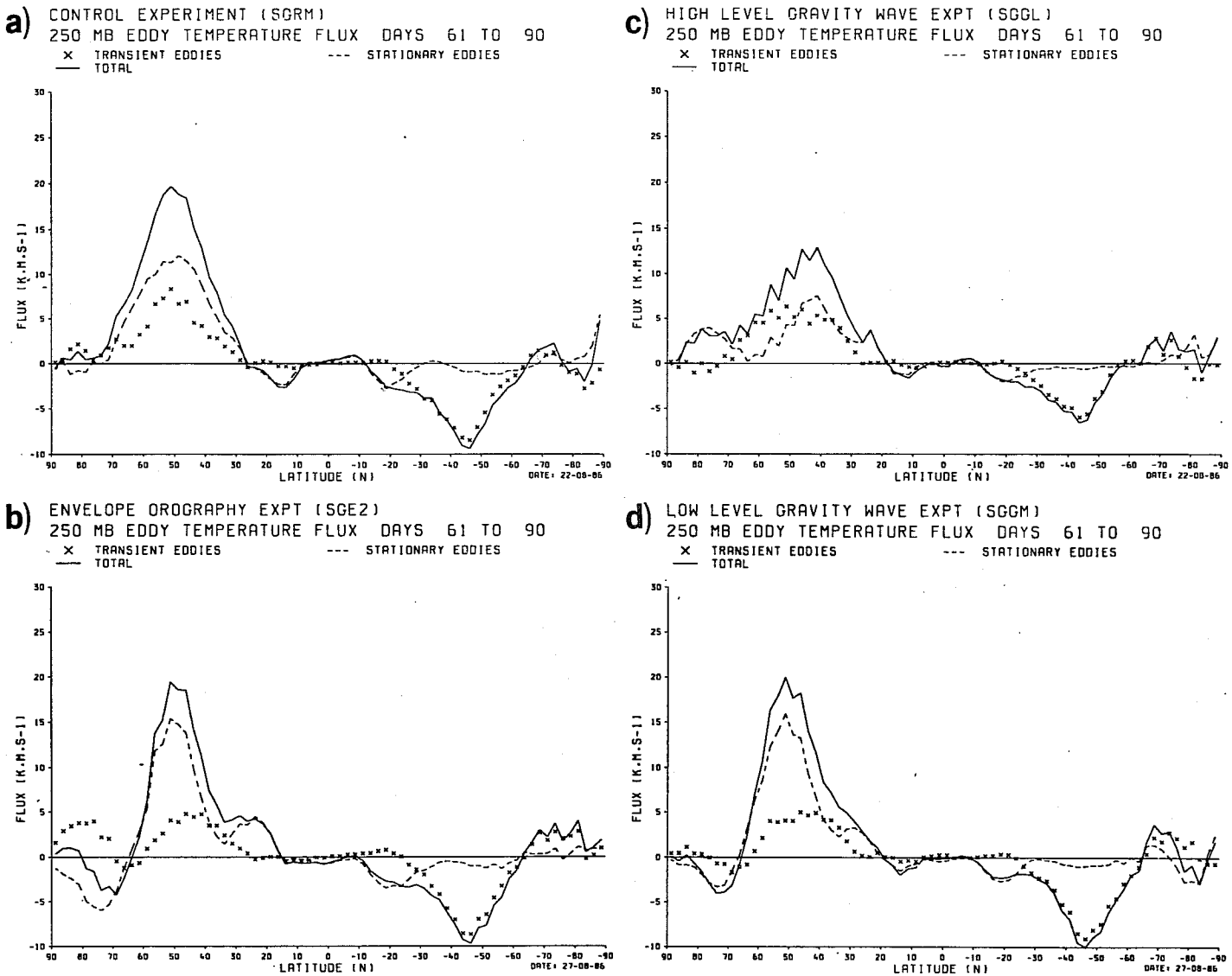

Fig. 11 Meridional heat fluxes $\overline{v''T''}$ (proportional to the vertical component of the Eliassen-Palm flux) from the UKMO climate model (90-day wintertime with $2\frac{1}{2}$x$3\frac{3}{4}$° resolution) a) mean orography b) 2σ envelope orogrpahy c) high-level 'thermal' drag d) low-level 'thermal' drag

whether the stress is absorbed at the bottom or at the top of the model (cf Lilly, 1972). This is consistent with the fact that the surface wind is determined, for given depth-averaged horizontal momentum flux, by the magnitude of the surface stress rather than its distribution in the vertical. However, there are some important differences between the upper and lower-level drag experiments, particularly in the zonal wind cross-section and in the 200mb height distribution. One can observe that the distribution of winds in the low-level drag experiment is similar to that in the envelope orography experiment, with a fairly uniform meridional shear in the upper troposphere. Furthermore, with low-level drag the winds are too strong in the mid-latitude upper troposphere. The distribution of zonal winds in the upper-level drag experiment, on the other hand, is more realistic, with strong meridional wind shears just poleward of the sub tropical jet and weaker shears further poleward. At lower altitudes the zonal wind is also well simulated in the upper-level drag experiment. With low-level drag, the shape of the 200mb flow is quite realistic (Fig 10b), but, consistent with the zonal wind cross-section, the winds in high latitudes are too strong. In the upper-level drag experiment some of the stationary-wave features, such as the Rockies ridge and Canadian trough, have insufficient amplitude (Fig 10c).

As shown in Fig 11, in both the low-level drag and envelope orography runs, stationary meridional heat fluxes are increased compared with values for the integration with mean orography only. This suggests that in both of these experiments the orographic parametrizations excite enhanced vertically-propagating Rossby waves. The reduction in upper-level zonal-mean flow in these runs may be associated with the dissipation of these Rossby waves near the top of the model. It would appear, then, that the low-level

drag acts in many ways as an envelope orography (as Tibaldi, 1987, predicted would occur). The upper-level drag experiment appears to have corrected the zonal-mean flow bias, but at the expense of the stationary wave stucture.

The experiments above suggest that an accurate climatological simulation might be attained with some judicious combination of upper-level and low-level drag. It would be hopelessly contrived to try some ad hoc combination; however, suffice it to say that at this stage we have reached a position where the GWD parametrization can be thought of as an immediate extension of the above ideas and as a means of achieving just such a combination in a reasonable, scientifically consistent and logical way.

3. THE PARAMETRIZATION SCHEME

On scales smaller than model resolution there exist gravity waves excited by stratified flow over irregular terrain. Depending on the atmospheric static stability and vertical wind shear, these waves can propagate vertically to great heights unless absorbed and/or reflected by critical layers, or unless they become unstable to convective or shear instabilities (i.e. the gravity waves can break). The Eliassen-Palm theorem implies that in steady conditions wave stress ($\underset{\sim}{\tau}_{gw}$) = $\overline{\rho u'w'}$, is independent of height until dissipation of wave energy occurs (Bretherton 1969, see also Booker and Bretherton (1967), Lindzen (1981) etc.)

The influence of these gravity wave stresses on the large-scale flow occurs in regions of wave momentum flux divergence, that is

$$\left(\frac{d\hat{v}}{dt}\right)_{gw} = - g \frac{d\hat{\tau}}{dp}\,gw \qquad (1)$$

The formulation of a parametrization scheme for GWD therefore consists of two basic parts;

(a) the parametric form for $\underset{\sim}{\tau}_{gw}(x,y)$ at the "surface" which determines the lat./long. distribution, and

(b) the modelling of the dissipation/absorption processes which determine the vertical distribution $\underset{\sim}{\tau}_{gw}$.

Only sufficient algebra is given here to understand the implementation of the scheme, the detailed derivation is given in Shutts, (1986) and Palmer et al. (1986).

3.1 Gravity wave stress at lower boundary $\underset{\sim}{\tau}_{g,w}$

Linear wave theory with sinusoidal topography suggests the form

$$\underset{\sim}{\tau}_{gw} = \frac{1}{2}\rho_s |\underset{\sim}{V}_s| \underset{\sim}{V}_s \nu \lambda \overline{h'^2} \qquad (2)$$

where suffix 's' is nominally the "surface", $\overline{h'^2}$ is a measure of the sub-gridscale orographic forcing (e.g. the sub-gridscale variance) and λ is a characteristic wavenumber for the gravity-wave producing orography ($\sim 10^{-4}\ m^{-1}$). The vertical wavenumber is given by

$$\nu = \left\{ \frac{N^2}{|\underset{\sim}{V}|^2} - \frac{1}{|\underset{\sim}{V}|} \frac{d^2 \underset{\sim}{V}}{dz^2} - \lambda^2 - \frac{1}{4H_o^2} \right\}^{\frac{1}{2}}$$

where $N^2 = g\frac{d}{dz}\ln\theta$ and $H_o = [-\frac{d}{dz}\ln\rho]^{-1}$.

Considerable simplification results for typical atmospheric values since $N^2/|\underset{\sim}{V}|^2$ >> other terms. Hence

$$\nu \approx N/|\underset{\sim}{V}| \text{ and } \underset{\sim}{\tau}_{gw} \doteq \rho_s K N \underset{\sim}{V}_s |h'|^2 \qquad (3)$$

where $K(\sim\frac{1}{2}\lambda)$ represents a 'tuneable' parameter related to the sub-gridscale orographic spectrum and the choice of definition of N, V_s and h', but is of order 10^{-4}-10^{-5} m^{-1}. Typical atmospheric values with h' = 200 m and $K = 2.5\times10^{-5}$ gives $\tau_{gw} \sim 0.1$ N/m^2 (or 1 dyne/cm^2) so this is a significant atmospheric stress. It can be seen that this gravity wave stress is highly variable geographically through h'(x,y) but also geographically and temporally variable through the product of N and V_s.

3.2 Vertical structure of τ_{gw}

As stated previously, the variation of stress with height depends on the processes by which the momentum flux associated with the vertically propagating waves is absorbed by the mean flow. There is considerable observational evidence (see this volume) that, both in the boundary layer and in the lower stratosphere, gravity waves become convectively unstable and break, generating turbulence. Since the waves amplify as $\rho^{-\frac{1}{2}}$, the local Richardson number can fall below 1/4. This is not the mean flow Richardson number ($\bar{R}$) but a 'wave' Richardson number ($\tilde{R}$) and it is the value of this that determines the onset of turbulence. Palmer et al. use this concept in their scheme to determine the levels at which the gravity wave stress is dissipated. As discussed by Lindzen (1981), it is assumed that in regions of instability the wave amplitude decreases until marginal stability is achieved, that is $\tilde{R} \geq \tilde{R}_{CRIT}$, (see later).

3.3 The 'wave' Richardson number ($\tilde{R}$)

As derived by Shutts, $\tilde{R}$ follows from the two-dimensional stratified flow theory of Long (1954). The important result here is that the horizontal component of vorticity in a flow displaced vertically (e.g. over a mountain)

is related to undisturbed parameters upstream, hence a local shear can be defined as

$$\left|\frac{d\hat{u}}{dz}\right| = \left|\frac{\overline{du}}{dz}\right| + \left|\frac{N^2}{\bar{u}}\right| |\delta z|$$

where δz is the vertical displacement.

For a sinusoidal wave field (vertical wave number ν) it can readily be shown that the local static stability has a minimum value $B_{min} = \bar{B}\,(1-\nu|\delta z|)$, thus

$$\hat{R} = \frac{N^2(1-N|\delta z|/\bar{u})}{\left\{\left|\frac{d\bar{u}}{dz}\right| + \frac{N^2|\delta z|}{|\bar{u}|}\right\}^2} \qquad (4)$$

which can be written

$$\hat{R} = \frac{\bar{R}(1-\alpha)}{(1+\bar{R}^{\frac{1}{2}}\alpha)^2} \qquad \text{where} \quad \alpha = \frac{N|\delta z|}{\bar{u}} \qquad (5)$$

A number of assumptions have been made in this derivation, including a mixture of non-linear and linear theory, and the neglect of the phase difference between the locations of minimum static stability and maximum shear (partially justified by considering an ensemble of phase incoherent gravity waves). However it does embody the main physics of the problem through the numerator (convective instability) and the denominator (shearing instability). It can readily be seen that $\bar{u} \to 0$ gives large α and hence small or negative $\hat{R}$, implying the onset of turbulent breakdown approaching a critical level.

3.4 Basic algorithm

The actual scheme is implemented in the following manner:-

(a) A 'low-level' flow $\underset{\sim}{V}_s$ is defined and the mean wind and static stability calculated.

(b) All reference to wind shear etc. is then taken in the plane of this 'low-level' wind vector.

(c) The 'surface' gravity wave stress is then computed as

$$\underset{\sim}{\tau}_s = K\rho_s N_s \underset{\sim}{V}_s |h'|^2 \qquad \text{with } K = 2.5 \times 10^{-5}\ m^{-1}$$

(see later for details about $|h'|^2$).

(d) This stress value is then assumed for the level above the 'low-level' flow and an implied wave displacement calculated using the general stress relationship

$$\underset{\sim}{\tau}_{k+1} = \underset{\sim}{\tau}_k = K\rho_k N_k |\underset{\sim}{V}_k||\delta z_k|^2 \text{ giving } \delta z_k = \left\{\frac{\tau_{k+1}}{K\rho_k N_k |\underset{\sim}{V}_k|}\right\}^{\frac{1}{2}} \qquad (6)$$

(e) This wave displacement is checked for stability and if $\tilde{R}$ is less than $\tilde{R}_{CRIT}$ (= 0.25), then a new value of $\delta z = (\delta z)_{CRIT}$ is computed from (5) with $\tilde{R}=\tilde{R}_{CRIT}$ (a simple quadratic solution).

(f) A new value of $\underset{\sim}{\tau}_k$ is now computed using (6) with $\delta z_k = (\delta z)_{CRIT}$.

(g) This procedure is then repeated for each level until either $\tau \to 0$ or the top model level is reached where $\tau_{k=1}$ is set equal to zero.

Equation (5) can be rewritten in the form

$$\tilde{R} = \frac{\bar{u}(\bar{u} - N|\delta z|)}{\{\bar{u}S/N + N|\delta z|\}^2} \text{ where } S = d\underset{\sim}{u}/dz$$

and it can readily be seen that $\tilde{R}_{CRIT}$ is reached as $N\delta z$ increases from zero towards $\underset{\sim}{u}$. Considering the calculation of $\tau(p)$, it is obvious that for

relatively small values of $\underset{\sim}{u}$, breaking will occur immediately above any significant orography (since $\delta z = h'$ until breaking occurs; typical values give $Nh' \sim 2\text{-}4$ m/s). For the major mountain ranges values of $h' \gtrsim 10^3$m are possible with widespread values in excess of 400m. The formulation of the sub-gridscale variances and the criterion for wave breaking are clearly fundamental and are discussed below.

3.5 Sub-gridscale orographic variance

The major contribution to the wave stress given by (3) is the orographic variance and, if $|h'|^2$ is simply the variance for a gridsquare, the wave stress is independent if wind direction (other than through directional correlations of N and $\underset{\sim}{V}_s$). This is an over-simplification since orography on most scales is highly anisotropic with pronounced nearly parallel ridges etc. To account for this basic effect, the sub-gridscale variance was computed as four directional components (E/W, N/S, NW/SE, NE/SW); this still ignores any anti-parallel effects but provides a much improved representation of stress. Fig. 12 gives examples of these directional variances. Flow parallel to major mountain ranges or plateaux no longer gives large wave stresses. The major ranges, nevertheless, present large variances to the incident flow, and typically these mountains act as a barrier to the flow, not necessarily as major gravity wave sources. Consequently the variance fields are reduced using simple dynamical criteria. The present operational scheme uses the relation

$$|h'|^2_{\text{effective}} = \text{Min}\ (|h'|^2,\ |h'|^2_{\underset{\sim}{R}})$$

where $|h'|^2_{\underset{\sim}{R}}$ is the solution of (5) with $\underset{\sim}{R}=\underset{\sim}{R}_{CRIT}$. Other criteria have been tested and are still being evaluated. Fig. 13 summarises the basic principles of the scheme.

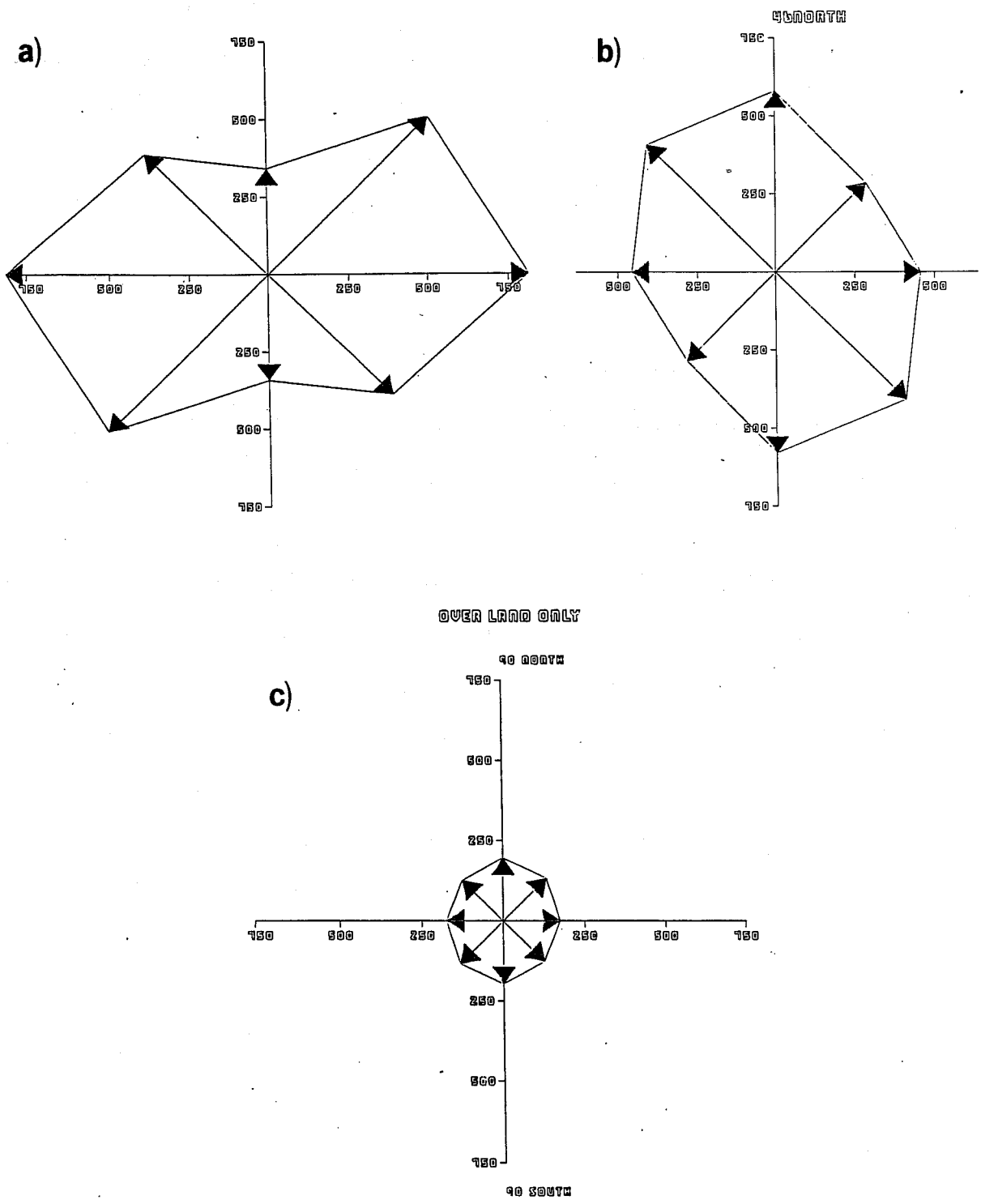

Fig. 12 The four components of subgridscale orographic standard deviation (in metres) for part of a) the Andes, b) the Alps, c) the Globe.

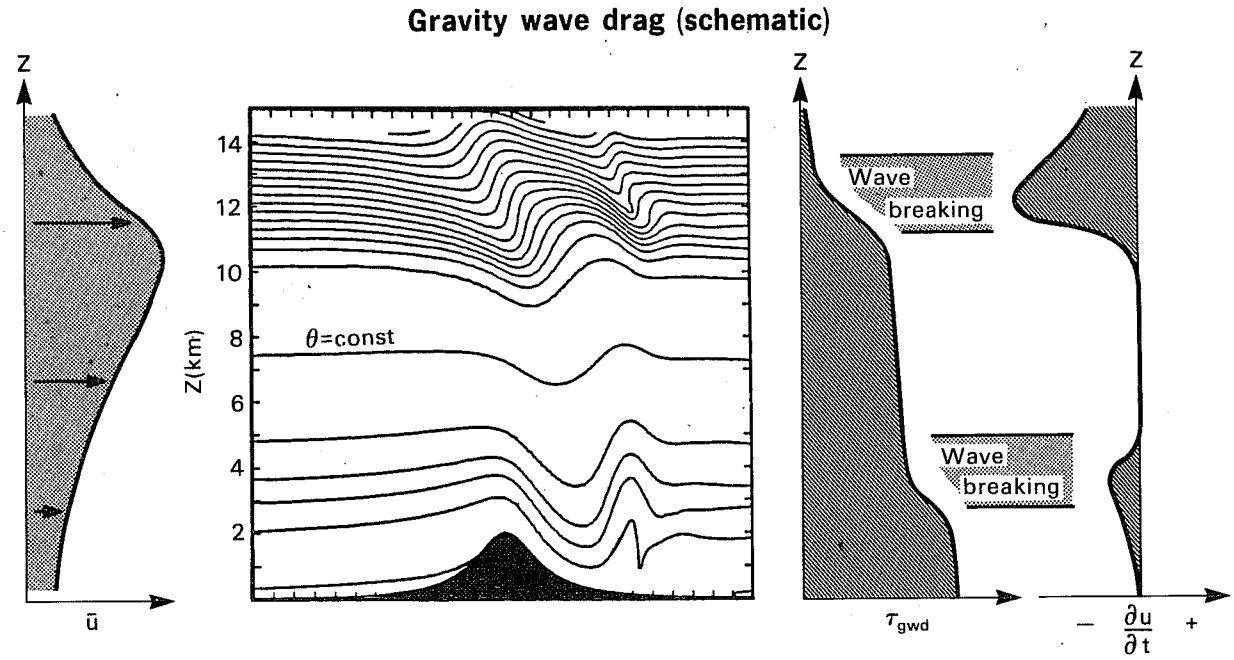

$\tau_{gwd} \propto N_{low} \left|V_{low}\right| \left|h'\right|^2$

$\left|h'\right|^2$ = Variance of sub-gridscale orography (directionally dependent)

Fig. 13 A schematic illustration of the gravity wave scheme.

3.6 Comments

As well as the assumptions made in the theoretical basis for the scheme, there are further choices to be made in the implementation; in particular, the definition of "low-level" wind and static stability is currently defined over the lowest three model layers (~500m) with the next layer above being the first at which waves can break. A precise definition of this flow over irregular terrain is clearly impossible, nevertheless it remains a rather arbitrary aspect of the scheme.

4. FORECAST EXPERIMENTS (10 DAYS)

4.1 T106L16 resolution

Twelve initial dates in the last 12 months were used with an envelope (one standard deviation) orography. No data assimilation with GWD was carried out. Fig 14a summarizes the mean scores for the northern hemisphere. This mean improvement over a year includes several summer cases with very little impact of GWD. There is a systematic improvement in all variables on all scales in all areas (as far as has been ascertained) from relatively early in the forecast and Fig 14b shows anomaly correlations for seven winter cases over Europe.

An ensemble verification of five winter cases shows the impact on zonal mean errors of the differing orographies (ENV and MEA) and the combination of gravity wave drag with the envelope (GWD). The improvements are marked (Fig 15) and correspond to a better zonal mean pressure distribution.

4.2 T106L19 resolution

Since 19-level forecasts have only been operational since 13 May 1986 and the major part of the 19-level forecast improvement is via the data assimilation,

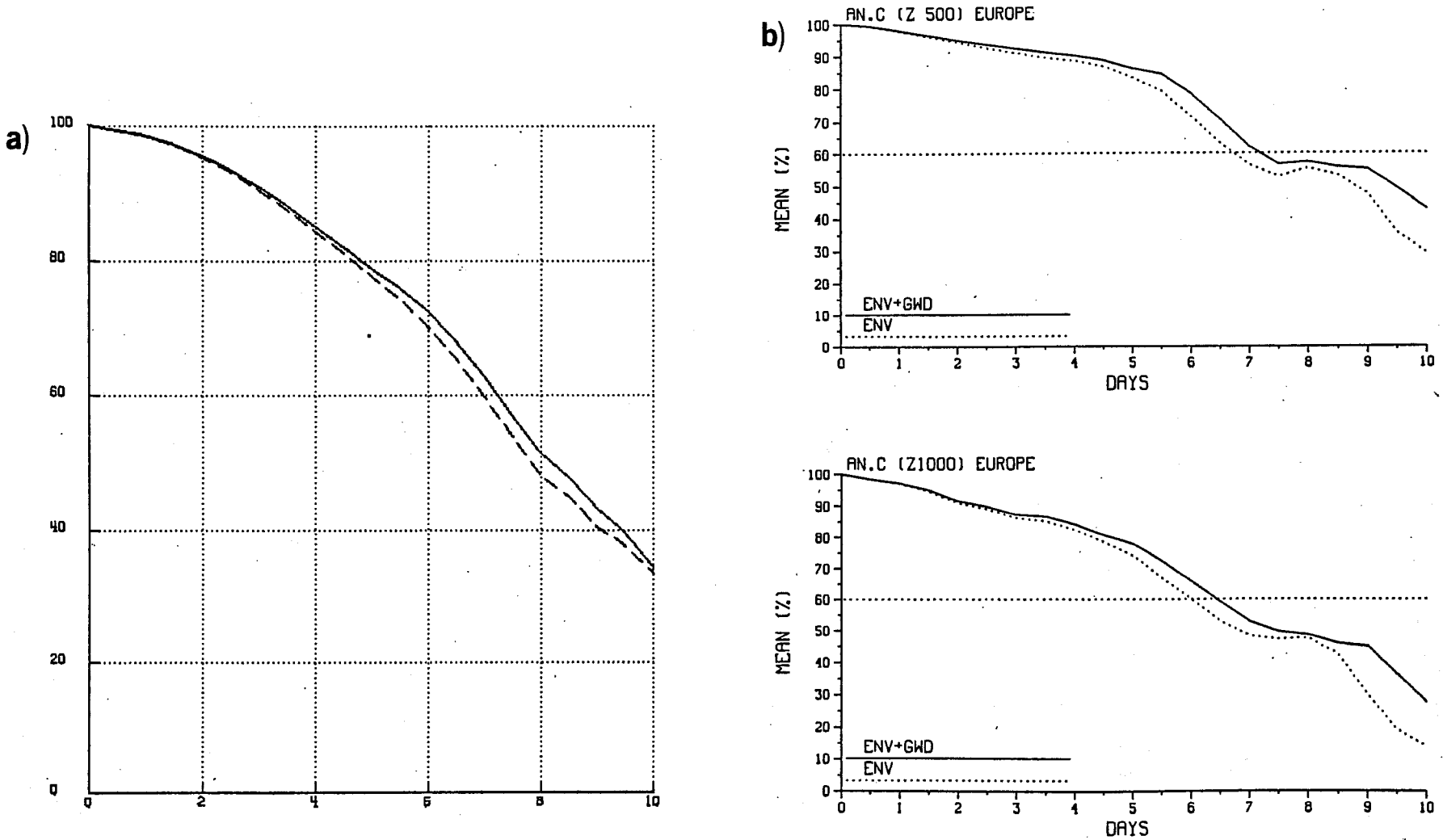

Fig. 14 a) Mean anomaly correlations for twelve T106L16 forecasts with and without gravity wave drag for the N. Hemisphere 1000 mb-200 mb heights.

b) Mean anomaly correlations of the 1000-200 mb heights for seven winter T106L16 forecasts for the European area.

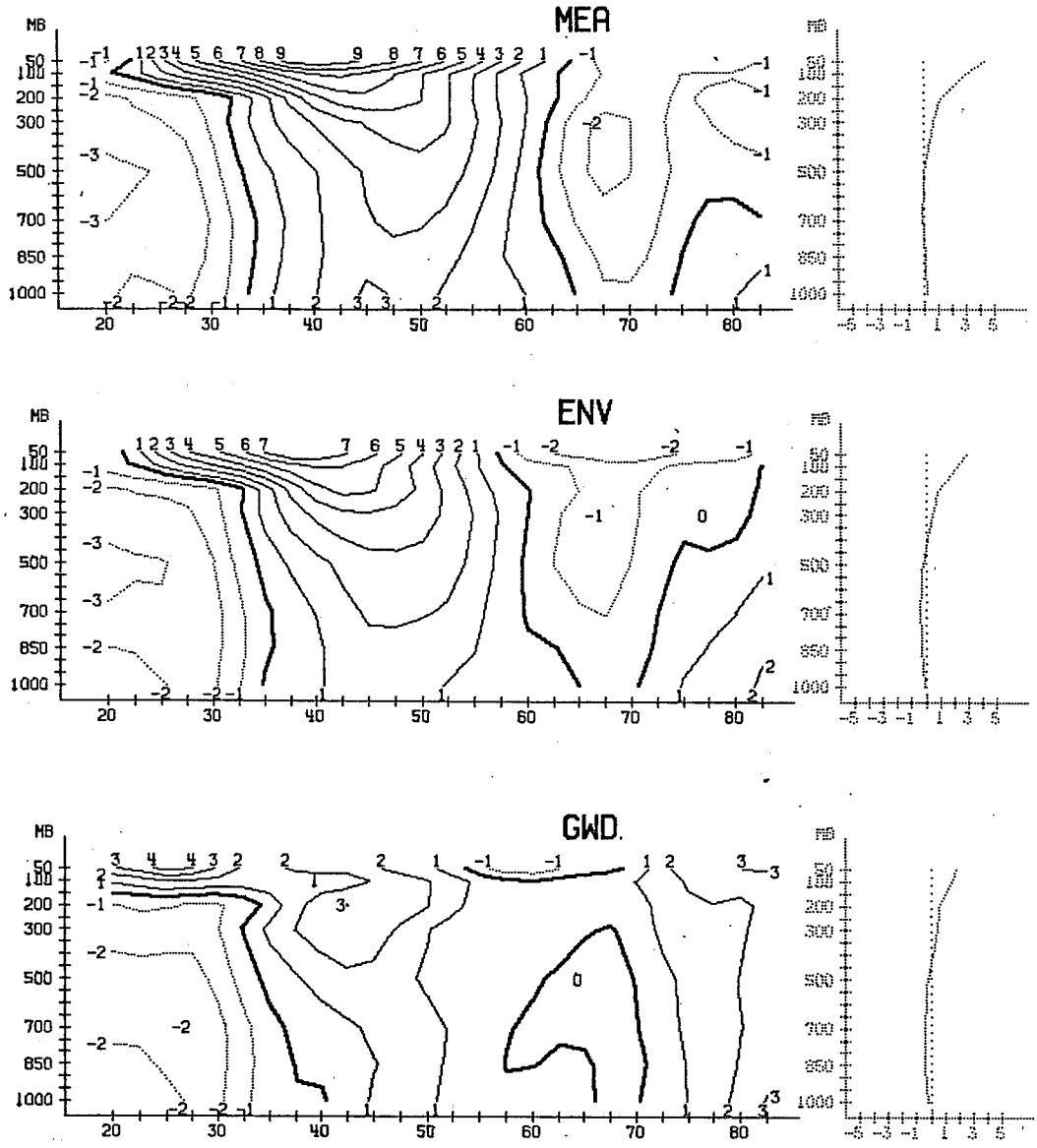

Fig. 15 Zonal mean wind errors (ms^{-1}) averaged over the second half of the seven winter T106L16 forecasts for mean orography (MEA), envelope orography (ENV) and envelope plus GWD (GWD).

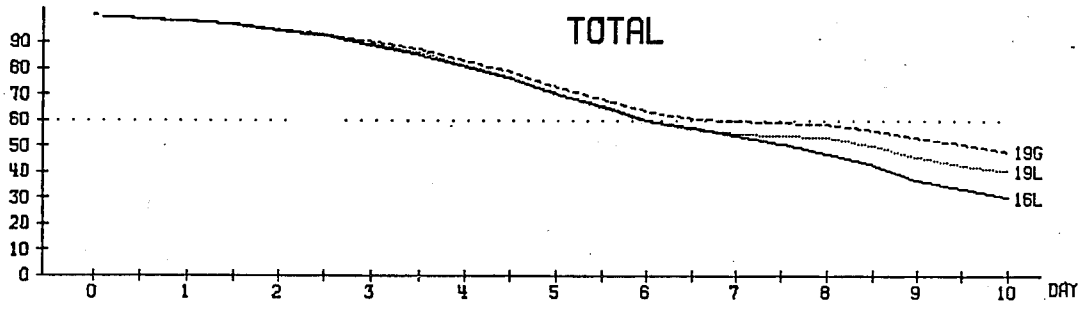

Fig. 16 Mean anomaly correlations of the 1000-200 mb heights for four T106L19 forecasts with (19G) and without (19L) GWD. Also shown are the corresponding scores for 16 level forecasts.

the potential for testing GWD was restricted to early summer only, when GWD is relatively weak. However, one six-day 19-level data assimilation had also been carried out for 24-30 March 1986 and a parallel assimilation was run with GWD included in the model cycling. This spring period has more gravity wave activity (although still less than in winter).

19-level forecasts with GWD were run from both six-day assimilations and compared to 19-level forecasts without GWD run from the original 19-level analysis and also to the then operational 16-level forecasts.

Fig 16 shows the mean scores for four forecasts run from 26, 28, 29 and 30 March 1986. Three further 19-level forecasts for 15 May, 11 April and 15 April 1986 give modest but consistent improvements (not shown) despite the summer minimum in gravity wave activity. It is clear that 19-level forecast improvements are enhanced with the addition of GWD, with a further improved stratosphere. Some synoptic examples of improved forecasts are discussed in the paper by Simmons in this seminar.

4.3 Remarks and further forecast experiments

Although the impact of GWD is significant, it is worth noting that globally the K.E. dissipation and stress due to GWD are less than 10% of their conventional frictional counterparts. Even if this comparison is limited to land areas the ratio is still less than 20%.

To confirm the importance of the geographical distribution of GWD, an experiment was run in which the GWD at any model latitude was distributed equally round the latitude circle. Fig 17 shows the objective scores and, despite a much improved zonal mean wind distribution, the forecast no longer benefits synoptically from the GWD.

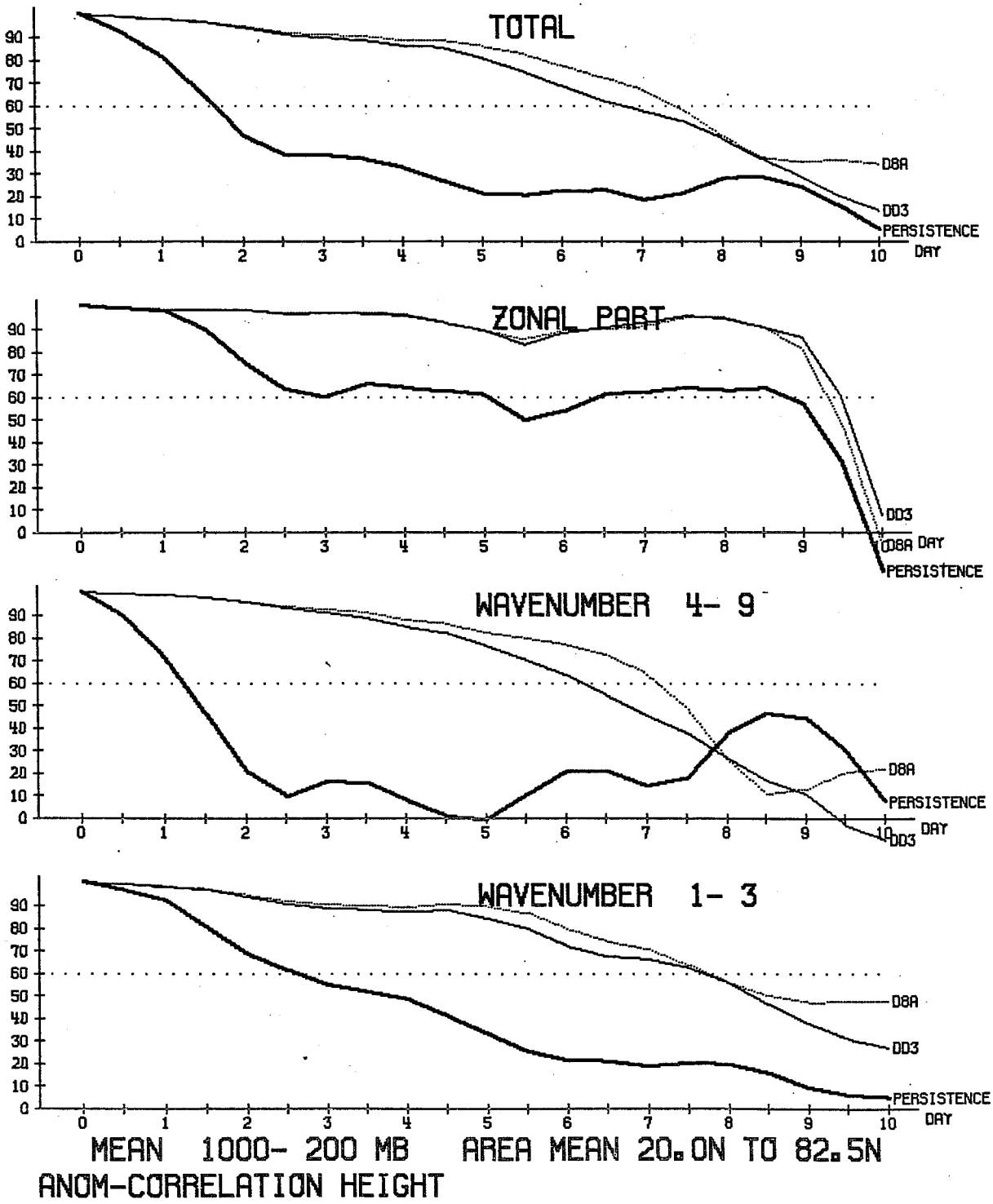

Fig. 17 The 1000-200 mb height anomaly correlation for a T106L16 forecast with zonal distributed GWD (see text) compared to normal GWD (dotted line).

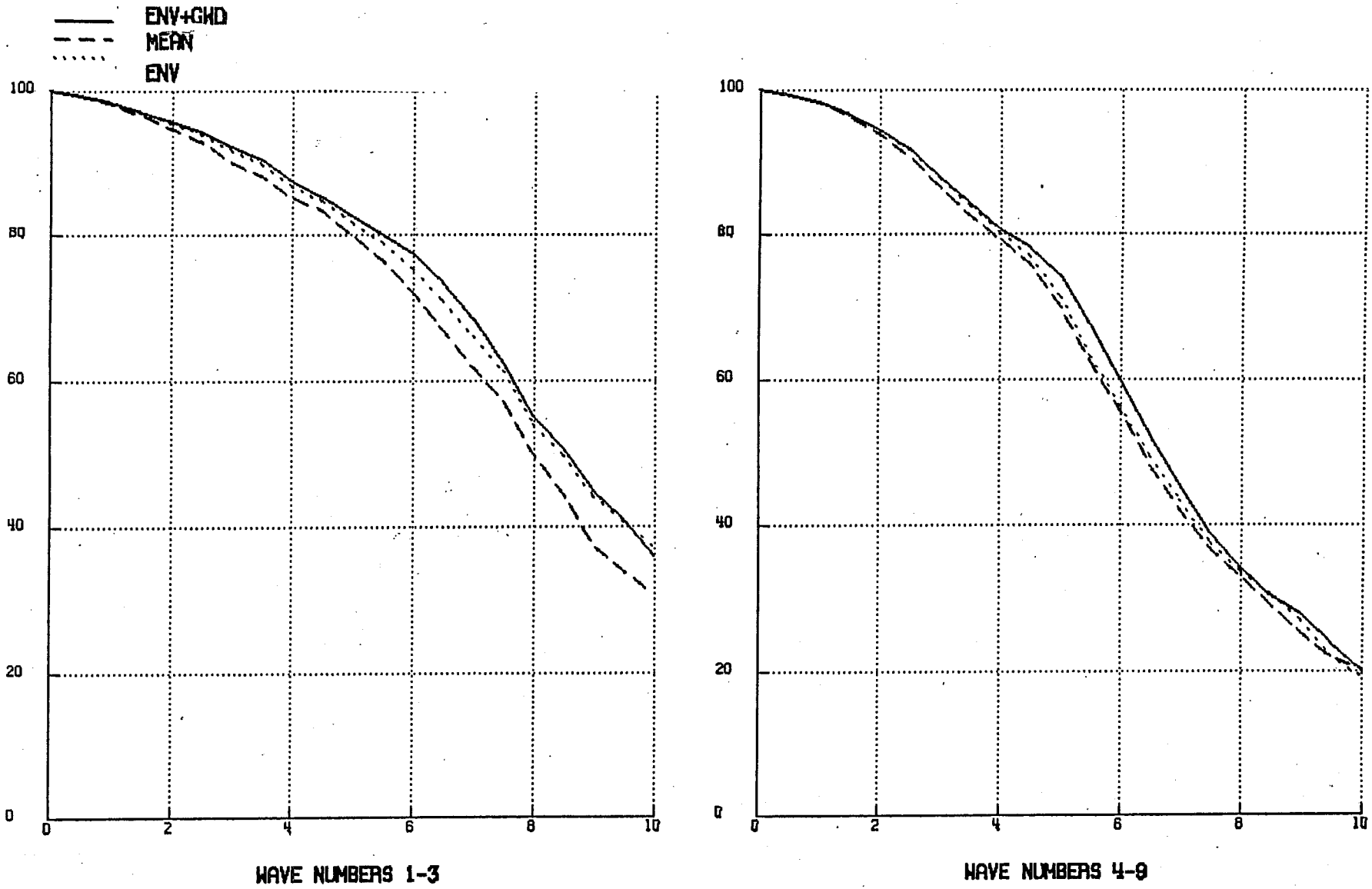

Fig. 18 Mean anomaly correlations of the 1000-200 mb heights for (1) envelope orography plus GWD, (2) mean orography and (3) envelope orography divided into long waves (1-3) and synoptic-scale waves (4-9).

Only forecast results for the northern hemisphere have been shown as the direct impact of GWD is small in the tropics and mostly small and unsystematic in the southern hemisphere where the effect of considerable wave drag around the Antarctic plateau is difficult to verify. The experimentation described in this section has been exclusively with the (one standard deviation) envelope orography; however, the set of T106L16 experiments was repeated with mean orography plus GWD and objective scores Fig 18 still indicate an advantage for envelope orography (plus GWD), albeit a much smaller one (a result consistent with the ECMWF seasonal integrations discussed in the next section).

5. IMPACT ON CLIMATE

We finally return to the problem of climate simulation, and examine the extent to which the GWD parametrization improves not only time-mean climate but also climate variability. This latter aspect is of particular importance for extended-range numerical weather prediction, as a model which cannot simulate accurately low-frequency variability cannot be considered a serious contender for long-range prediction.

In this section we describe a series of integrations from both the UKMO climate model and the ECMWF T42 model with identical parametrizations of gravity wave drag. This parametrization is essentially the same as described in Section 3, but differs in that a scalar orographic variance limited to a maximum of $(400m)^2$ was used. Various 90 day integrations using the same initial data as used in Section 2 form the basis of the discussion. In addition, we shall use some material from a set of multi-annual cycle integrations of the UKMO climate model described by Slingo and Pearson (1987).

Fig 19 shows the 90-day mean surface pressure field from integrations of both models with gravity-wave drag added to $\sqrt{2}\sigma$ envelope orography, and added to mean orography. In many respects, given the basic differences in model formulation, it is encouraging to find considerable similarity in the impact of gravity wave drag in the two models. With the GWD parameterization added to mean orography, both models show some weakening of the surface flow over Eurasia and North America, and hence significant improvement in the time mean PMSL field compared with the control integrations in (Fig 2b, c). On the other hand integrations of both models with GWD and $\sqrt{2}\sigma$ envelope orography show still further improvement in the mean PMSL field. Perhaps the most significant difference between the models is the depth of north Pacific pressure. It is not known whether such difference is statistically significant or due to sampling error.

In order to get some estimate of how much gravity wave stress is being generated in these experiments, Fig 20a shows the 90-day mean surface gravity wave fluxes in the ECMWF integration. Values of 0.4-0.6 Nm^{-2} over the Rockies and Alps are within estimates of pressure drag measured by microbarograph arrays (see elsewhere in this volume). The profiles of acceleration are shown in Fig 20b and they indicate substantial low-level wave breaking, again in agreement with observations.

Fig 21 shows the zonal-mean wind cross sections for UKMO and ECMWF models with GWD and envelope orography. Compared with climate, simulation of the subtropical jet and the lower stratospheric polar night jet is somewhat better in the UKMO integration than in the ECMWF integration. Both integrations show acceptable simulations of 200 mb height (Fig 22).

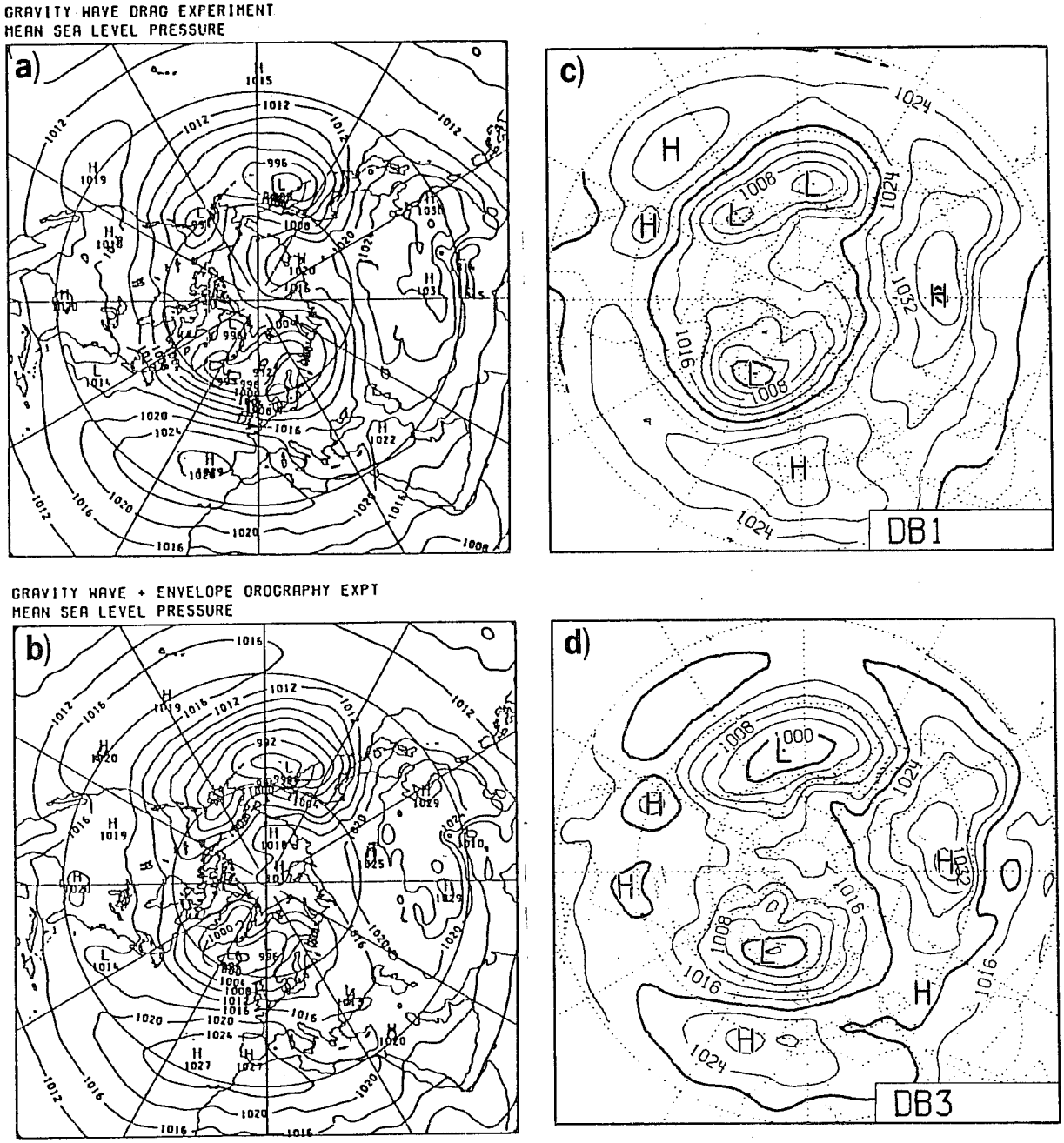

Fig. 19 90 day mean PMSL (mb)

a) UKMO mean + gravity wave drag
b) UKMO $\sqrt{2}\sigma$ envelope + gravity wave drag
c) ECMWF mean + gravity wave drag
d) ECMWF $\sqrt{2}\sigma$ envelope + gravity wave drag

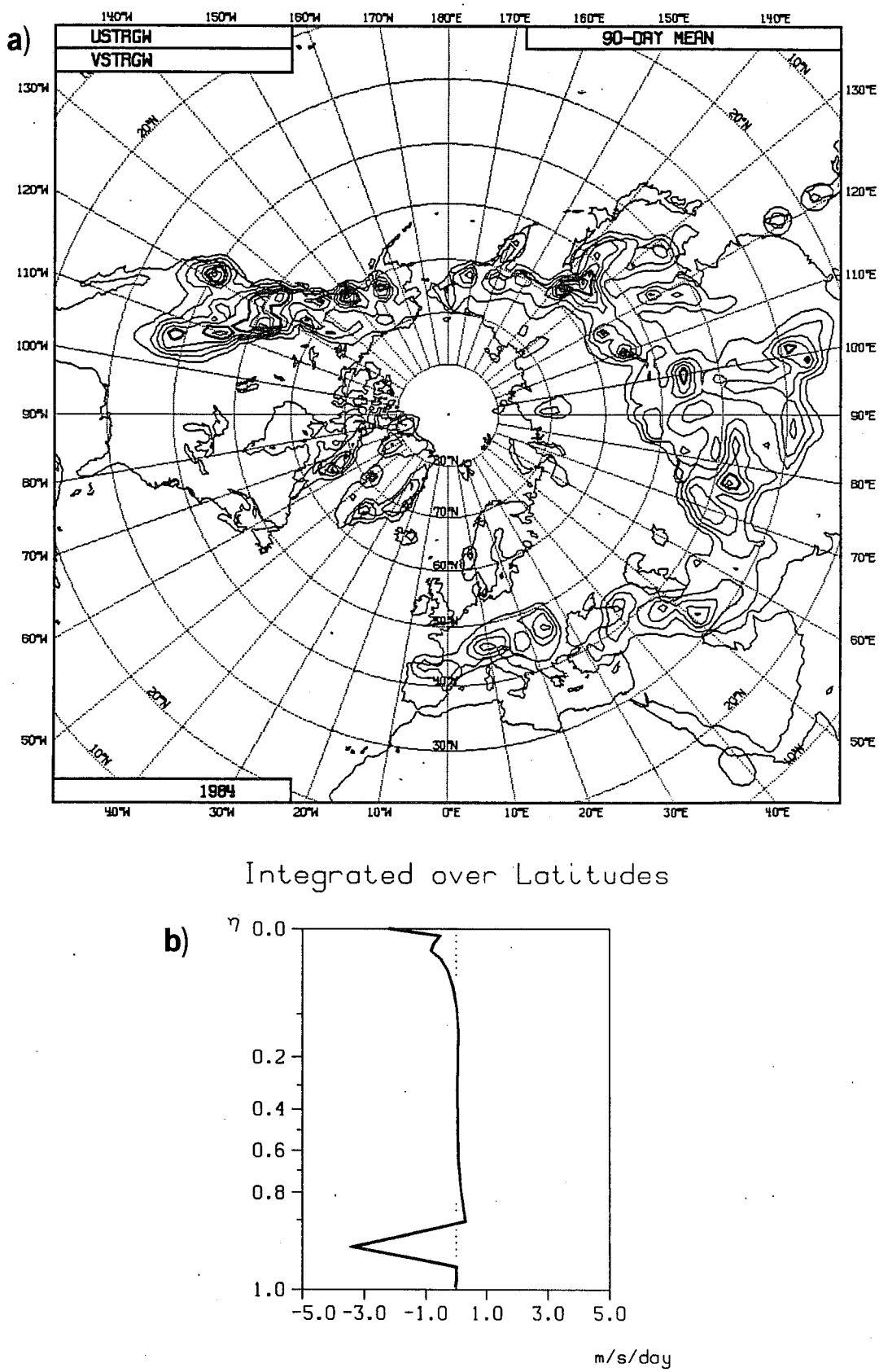

Fig. 20 a) 90 day mean stress due to gravity wave drag x 0 .1 Pa in ECMWF integration
b) 90 day mean tendency in the zonal direction due to gravity wave drag, averaged over all land point.

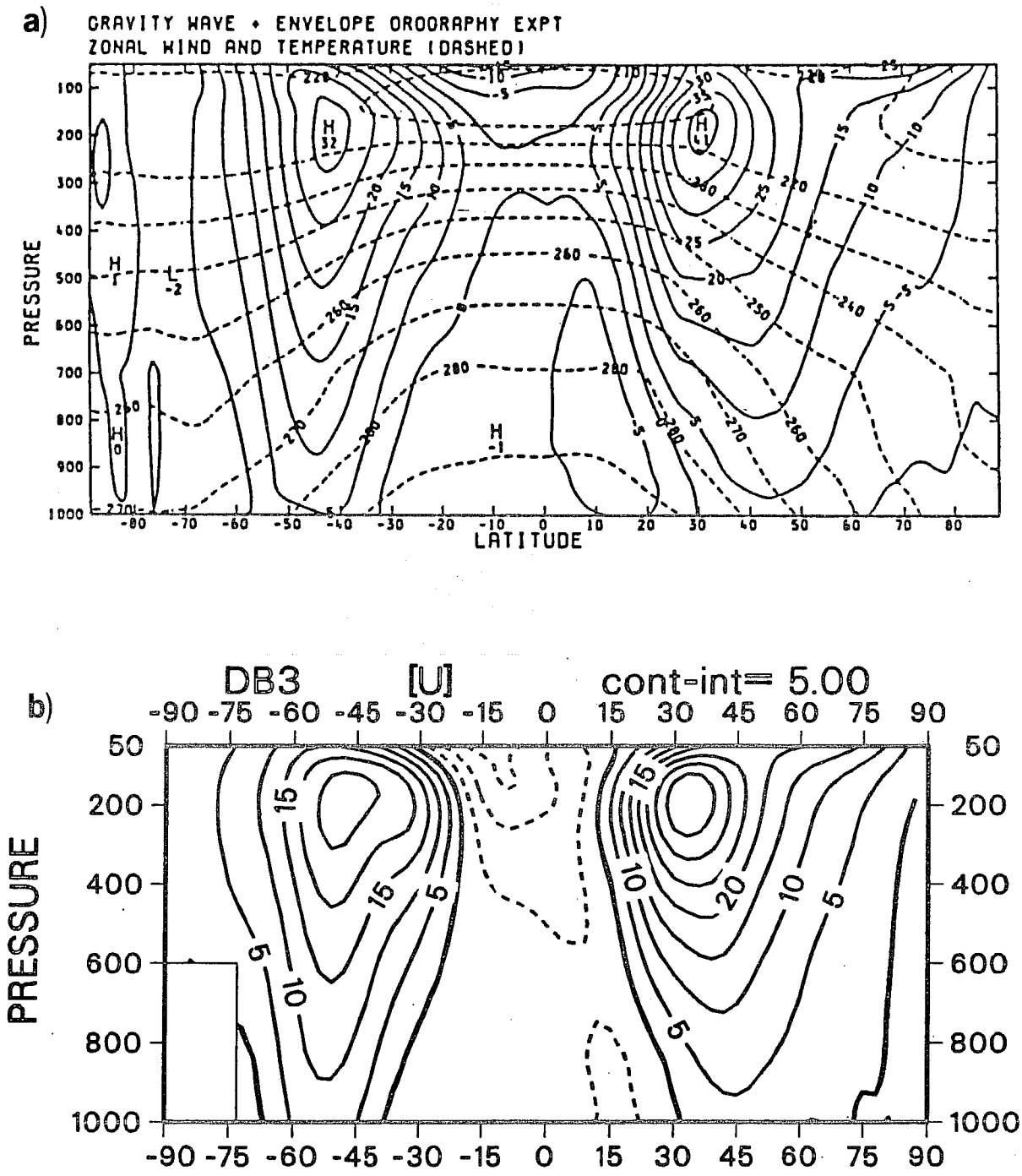

Fig. 21 90-day mean zonal mean wind cross sections (ms^{-1})
a) UKMO ($\sqrt{2}\sigma$ envelope + gravity wave drag)
b) ECMWF ($\sqrt{2}\sigma$ envelope + gravity wave drag)

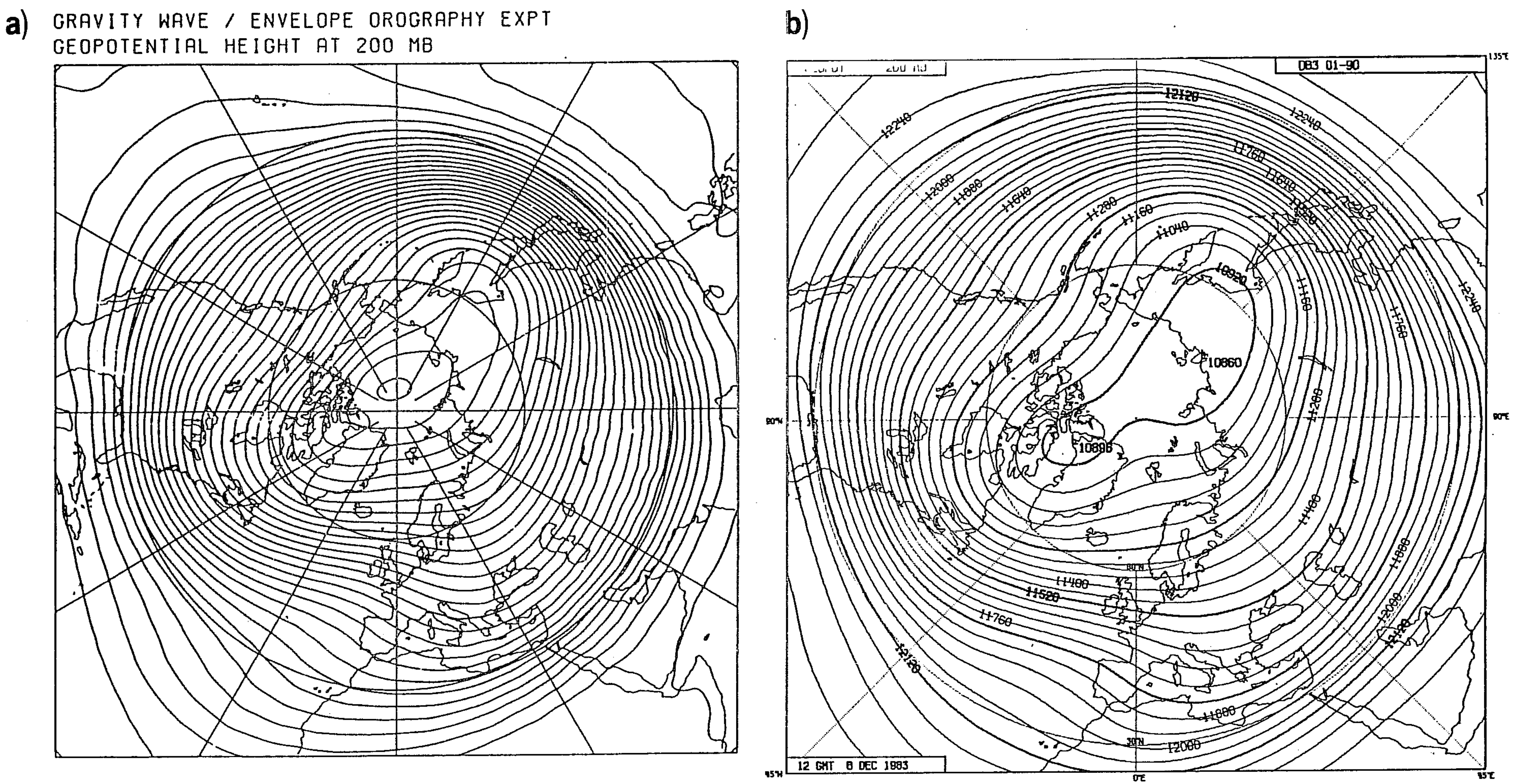

Fig. 22 As Fig.21 but for 200 mb height (dam)

In Fig 23 we show some further zonal mean cross-sections for the ECMWF integrations with mean orography (DB0), and envelope orography with GWD (DB3). Fig 23a, b shows the momentum and heat fluxes for zonal waves 1-3. It is clear that for DB0, momentum fluxes are too strong in the upper troposphere, whereas heat fluxes are too weak in the lower stratosphere. Both quantities are improved substantially in DB3.

This result appears to provide a rather nice example of the way in which the upper-level GWD by weakening the zonal mean winds, has improved the wave refraction properties of the mean flow, and allowed greater transmission of planetary-wave activity into the stratosphere, rather than equatorward refraction.

For the synoptic scale waves (zonal harmonics 4-9), both heat and momentum fluxes are too strong with mean orography; this is consistent with storm track activity being too intense (see below). Both these quantities are reduced in DB3, a little too much by comparison with observations. Again this appears consistent with the results below that storm-track activity is damped a little excessively over land.

It should be noted in passing that in all integrations of both the ECMWF and UKMO models, eddy kinetic energy is significantly weaker than observed. GWD neither improves nor worsens this systematic error. Preliminary diagnosis suggests that this error may be associated with an inadequately resolved tropopause.

As mentioned above, it is not sufficient to judge a model merely by its ability to reproduce time-mean climate; it must also be able to simulate

climate variability. In Fig 24, then, are shown both band-pass and low-pass filtered standard deviations of 1000mb geopotential height for the ECMWF model integration with envelope orography plus GWD. For comparison purposes, values for the integrations with envelope orography only, with mean orography only, together with climatological values, are also shown. (The climatological data is taken from Lau et al. (1981) with band pass and low-pass filters defined in Blackmon (1976). For the integrations, the filtered standard deviations are calculated by spectrally analysing the last 60 days of each integration, with band- and low- pass filters equivalent to those used on the observations.)

With mean orography, the band-pass filtered values show not only excessively strong storm tracks across most of the hemisphere but also quite incorrect positioning of maximum and minimum cyclonic activity (Fig 24a). With envelope orography only, storm-track activity is also too intense over the landmasses, and generally steered too far north (Fig 24b). This is consistent with results in Section 2, where the effect of envelope orography was to produce insufficiently diffluent jets, positioned too far north, over the main land masses. With GWD added to envelope orography, the storm tracks are correctly positioned, with maxima over the western part of the Pacific and Atlantic oceans (Fig 24c).

With both mean and envelope orography only, the maxima of low-pass variability are incorrectly positioned, particularly in the European sector (Fig 25a,b respectively). These errors are likely related to errors in the storm-track activity discussed above. The integration with GWD on the other hand, simulates low-frequency variability quite well with maxima of about the correct magnitude just to the west of the British Isles, and near the Aleutian Islands Fig 25c. Of course, to base these conclusions on just one set of

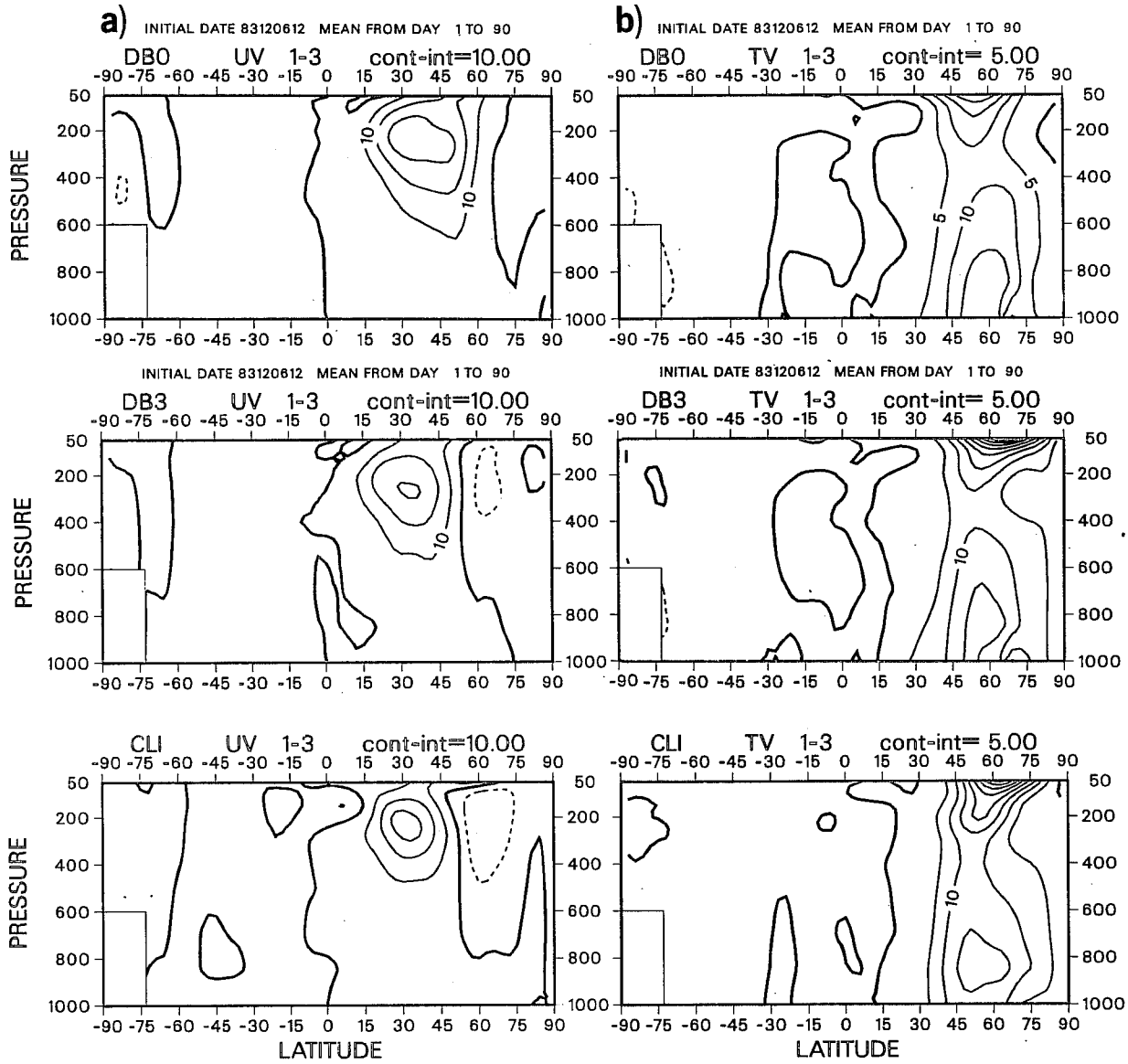

Fig. 23 90-day mean zonal cross-sections for the ECMWF integrations with mean orography, and $\sqrt{2}\sigma$ envelope + gravity wave drag
a) momentum flux $\overline{u'v'}$, waves 1-3 (m^2s^{-2})
b) heat flux $\overline{v'T'}$, waves 1-3 (mKs^{-1})

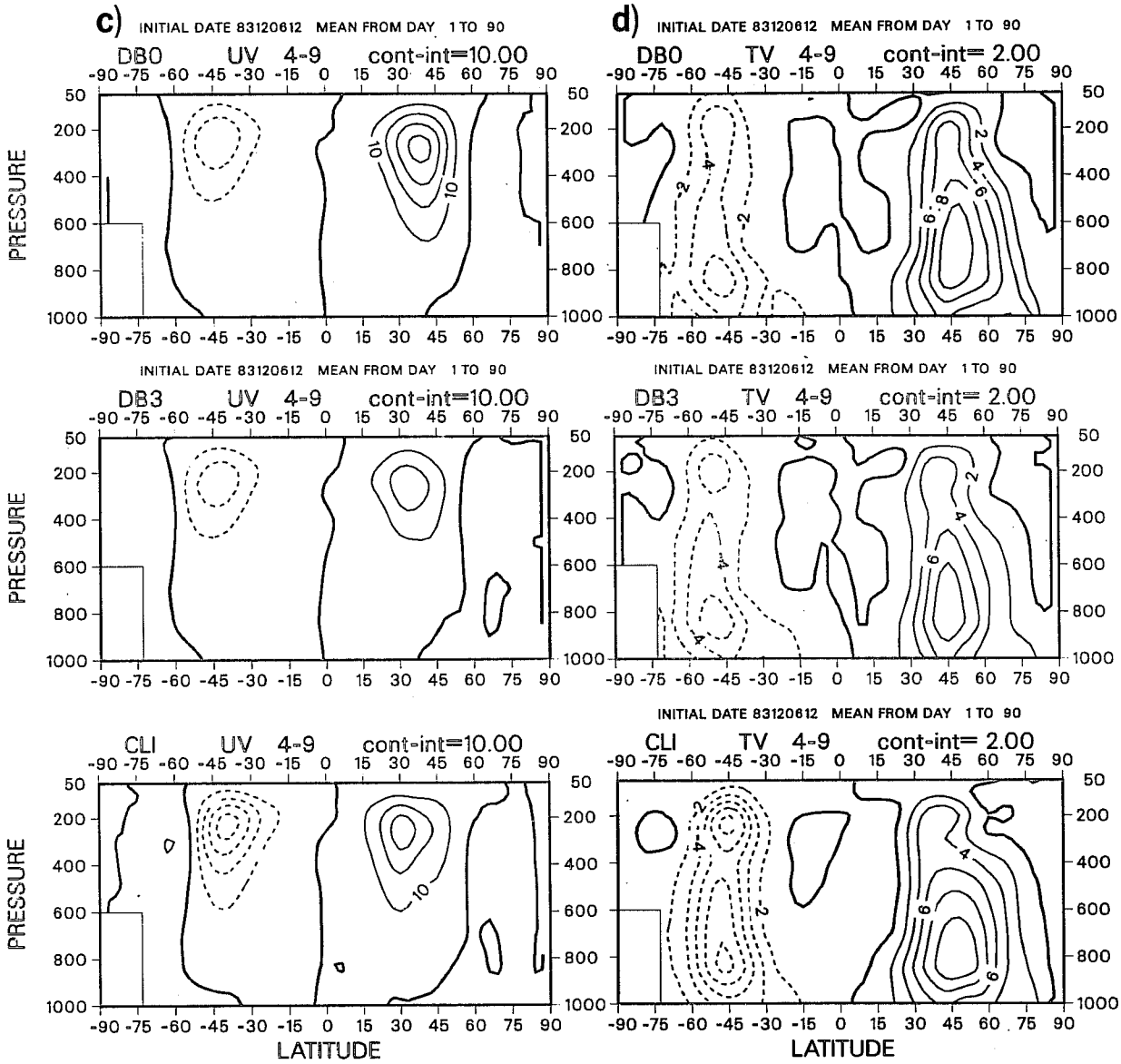

Fig. 23 (Cont) c) momentum flux $\overline{u'v'}$, waves 4-9 (m^2s^{-2})
d) heat flux $\overline{v'T'}$, waves 4-9 (mKs^{-1})

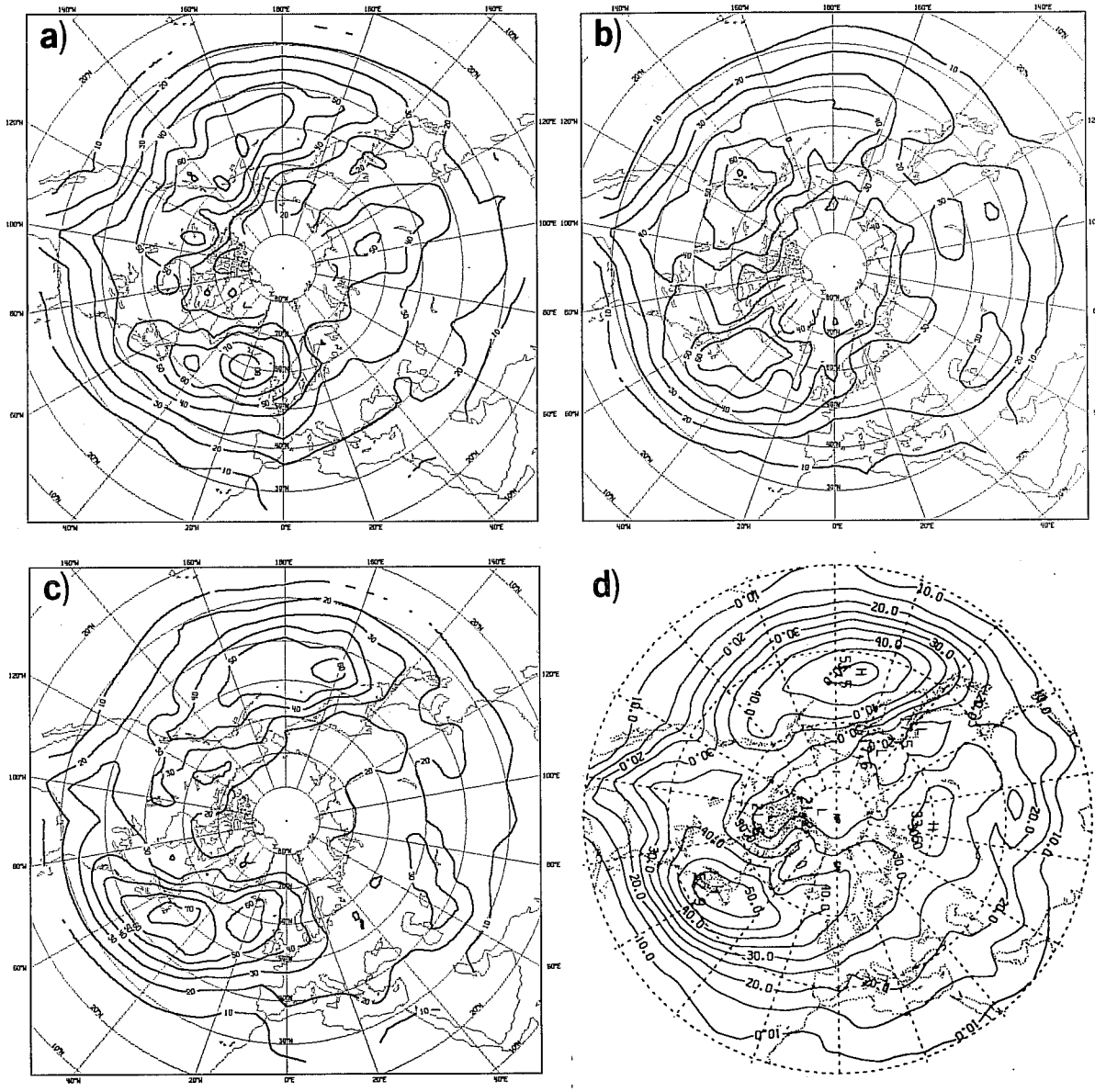

Fig. 24 Band-pass filtered standard deviation of 1000 mb height (m) (allowing fluctuations within 2-5 day range) from last 60 days of ECMWF integrations

a) mean orography
b) $\sqrt{2}\sigma$ envelope orography
c) $\sqrt{2}\sigma$ envelope orography and gravity wave drag
d) observed climate

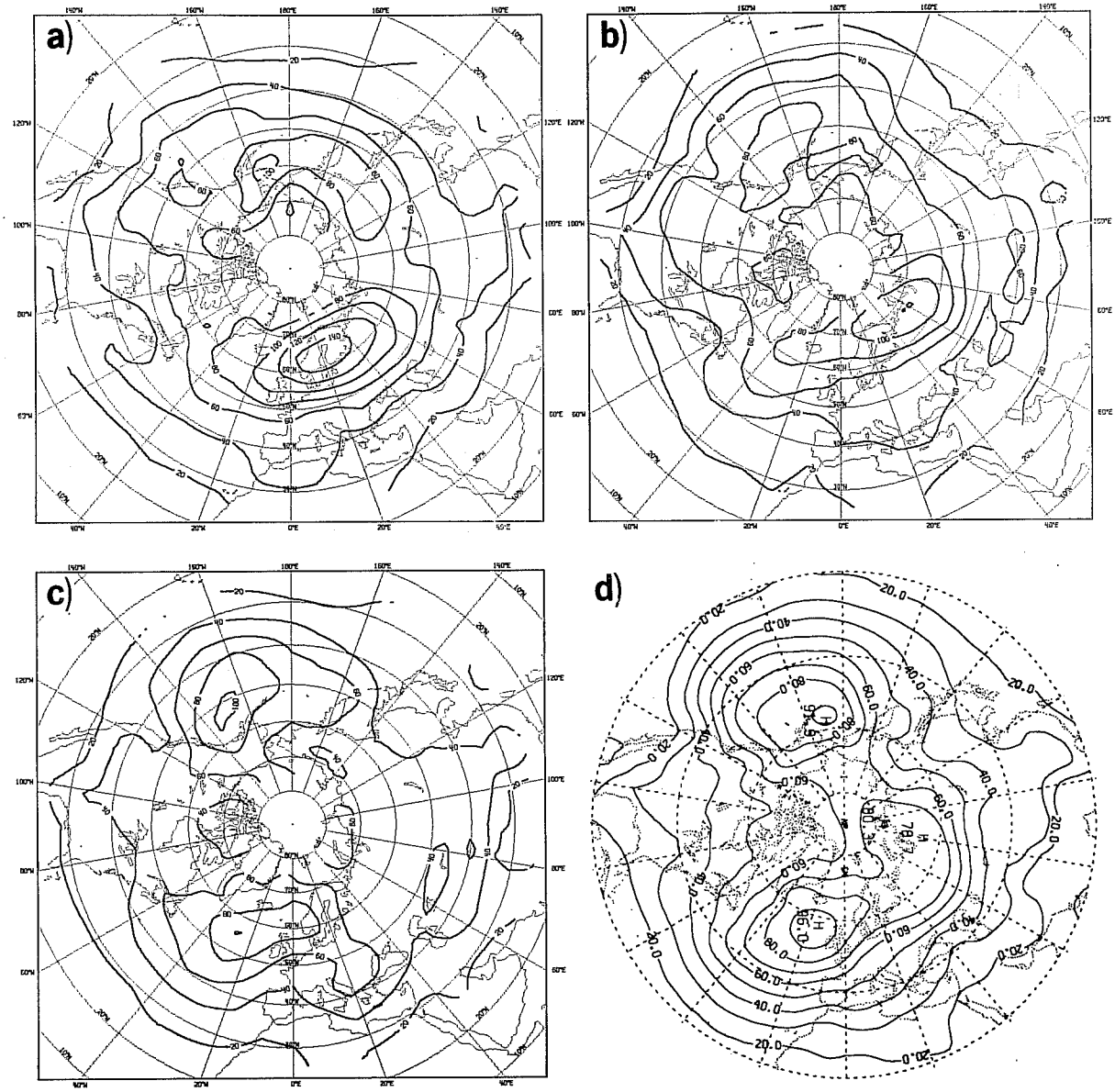

Fig. 25 As Fig. 24 but for low pass variability (fluctuations $\gtrsim$ 6 days).

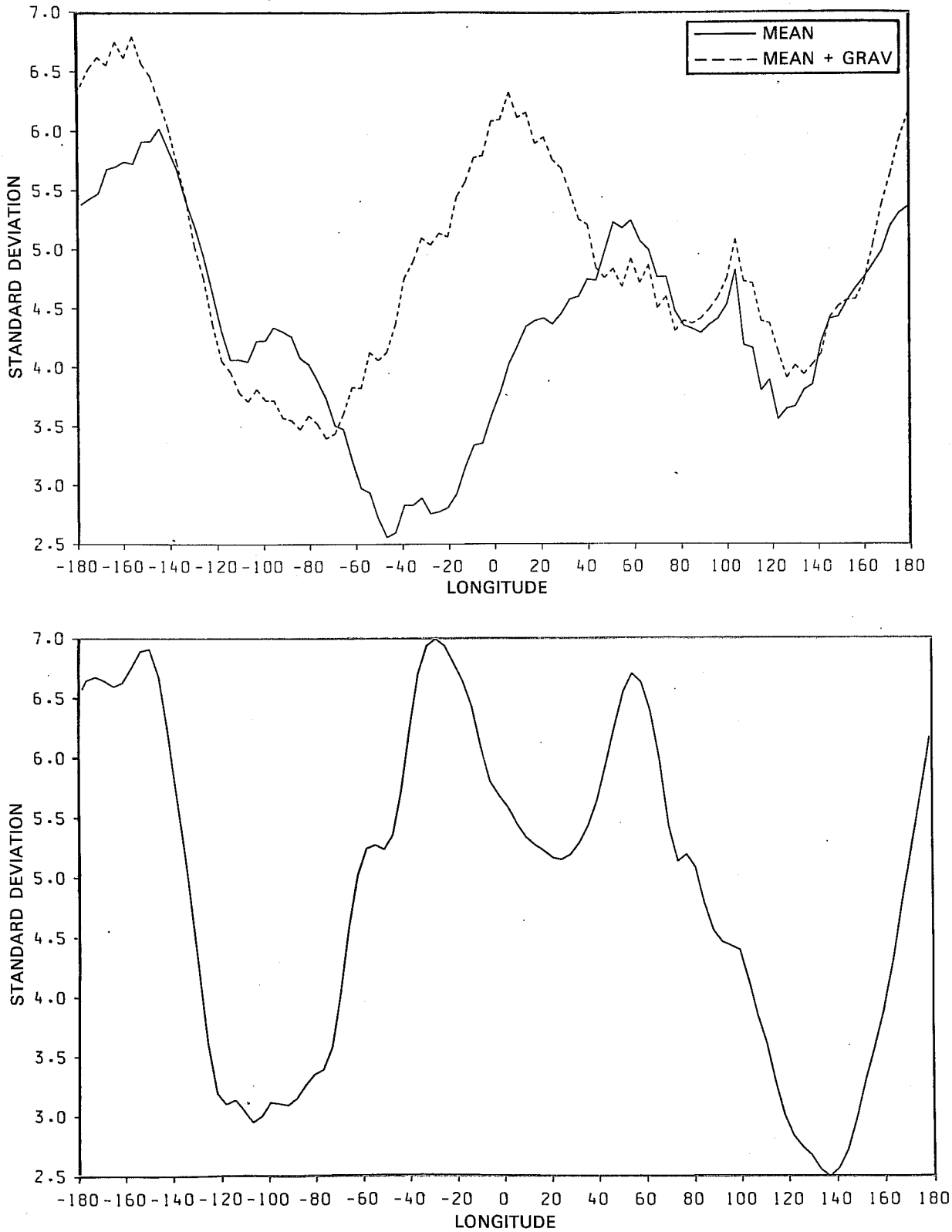

Fig. 26 Standard deviation of monthly mean surface pressure (mb), averaged from 90-30N over 4 winters of an annual cycle integration of the UKMO climate model with mean orography only (full line) and with gravity wave drag (dashed line).

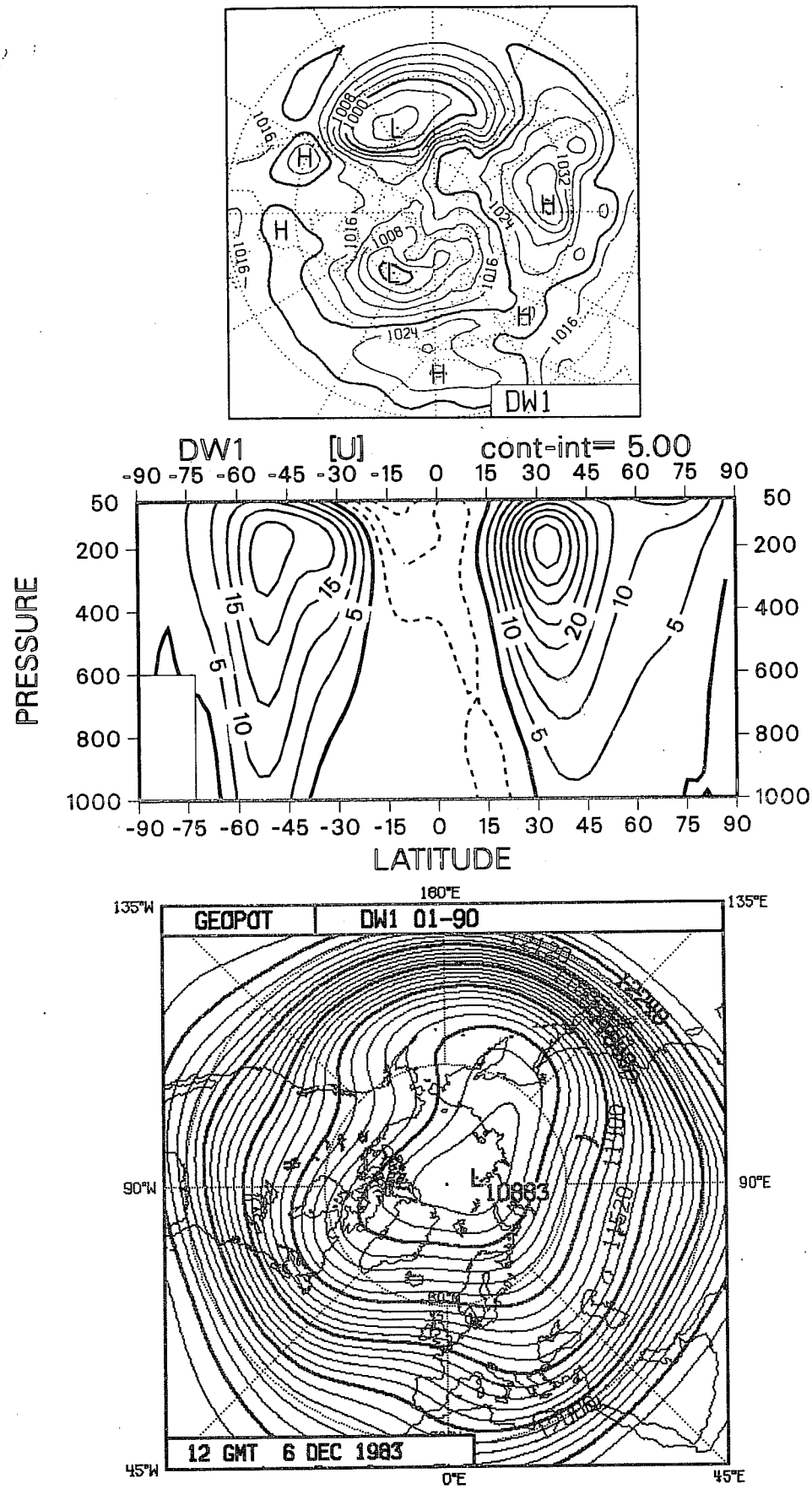

Fig. 27 90-day mean surface pressure (mb), zonal mean wind (ms^{-1}) and 200 mb height (dam) from T42 ECMWF integration with the operational version of gravity wave drag and $\sqrt{2}\sigma$ envelope orography.

90-day integrations would be somewhat unreliable, particularly for the estimates of low-frequency variance. However, they are largely consistent with results from the four-year integrations described by Slingo and Pearson (1987). For example, Fig 26 shows standard deviation of monthly mean surface pressure from twelve winter months of an integration with mean orography only, and with mean orography plus gravity wave drag. Values have been latitudinally averaged from 90°N to 30°N. It can be seen immediately that the major difference between the two curves is near the Greenwich meridian, where the integration with GWD has about twice as much monthly mean standard deviation as the run without. An observational estimate is also shown for comparison purposes.

Finally, in Fig 27, the 90-day mean PMSL, zonal mean wind cross-section and 200 mb height field are shown for a T42 integration with the operational version of the gravity wave drag scheme. The inhibition of low level drag is apparent with large reduction of zonal mean wind in the upper troposphere and lower stratosphere compared with that in Fig 21b. The 200 mb height shows, compared with Fig 22b, somewhat weaker stationary wave activity. This is particularly apparent in the stratosphere (not shown). In general the differences between this integration and that with the $(400\ m)^2$ variance cut-off are similar to the idealised integrations shown above with pure low level drag and pure upper level drag.

6. CONCLUSIONS

The general problem of representation of orographic forcing in numerical models has been considered, with particular emphasis on the drag effect of sub-gridscale orography on scales where gravity wave motions are significant.

Purely from model simulations, it has been argued that with improving resolution there are major deficiencies in the global angular momentum budgets such that the balance of eddy flux convergence of westerly momentum by frictional drag and large scale mountain torque is only obtained by excessively strong zonal flows.

Possible 'cures' such as enhanced surface roughness or enhanced large-scale orography which increase that drag are considered, and it is concluded that these are insufficient to alleviate the general problems.

A systematic argument has been presented which leads logically to a basic stress formulation due to gravity waves excited by stratified flow over irregular terrain. The results discussed use a parameterization based on that of Palmer et al. (1986). This scheme has been improved by introducing directionally-dependent subgrid-scale orographic variances. A substantial set of medium-range forecast experiments show significant improvements in forecast skill and reduction in model systematic errors, with particular improvements in the life-cycles of baroclinic waves.

Comparisons between ECMWF and UKMO model simulations for a 90-day winter period using models of similar resolution identified similar deficiencies without GWD representation and similar marked improvements when the parameterization scheme was included. In particular, the virtual elimination of the excessive westerly flow over the continents is associated with better located storm tracks and improved low frequency variability.

The problem remains of understanding and modelling the relationship between the large-scale orographic representation (e.g. mean, envelope) and the wave drag.

The use of idealized stress profiles, whereby the wave drag is limited to either the lowest levels only or the uppermost levels only, suggests that the impact of the low-level drag has some similarity to that of an envelope orography. Results from two-dimensional theoretical and explicit mountain wave models together with observational studies confirm that very large drags can occur in the troposphere rather than the stratosphere. Future work will need to reconcile such evidence with the model orographic representation of flow blocking (barrier) effects, three-dimensional aspects and the wave drag itself.

References

Booker, J.R. and F.P. Bretherton, 1967: The critical layer for internal gravity waves in a shear flow. J.Fluid Mech., 27, 513-539.

Bretherton, F.P., 1969: Momentum transport by gravity waves. Quart.J.R.Met.Soc., 95, 213-243.

Charney, J.G and P.G. Drazin, 1961: Propagation of planetary scale disturbances from the lower into the upper atmosphere. J.Geophys.Res., 66, 83-109.

Cubasch, U., 1981: The performance of the ECMWF model in 50 day integrations. ECMWF Tech.Memo.No.32.

Hoskins, B.J., M.E. McIntyre and A. Robertson, 1985: On the use and significance of isentropic potential vorticity maps. Quart.J.R.Met.Soc., 111, 877-946.

Jeffries, M., 1933: The function of cyclones in the general circulation (reprinted in 'Theory of thermal convection', ed. Barry Saltzman, 1962, Dover Publications Inc).

Lilly, D.K. 1972: Wave momentum flux - a GARP problem. Bull. Am. Met. Soc. 53, 17-23.

Lindzen, R.S., 1981: Turbulence and stress due to gravity wave and tidal breakdown. J. Geophys. Res., 86, 9707-9714.

Lindzen, R.S., 1985: Multiple gravity-wave breaking levels. J.Atmos.Sci., 42, 301-305.

Long, R.R., 1953: Some aspects of the flow of stratified fluids. I. A theoretical investigation. Tellus, 5, 42-58.

Manabe, S., and D.G. Hahn, 1981: Simulation of atmospheric variability. Mon.Wea.Rev., 109, 2260-2286.

Palmer, T.N., G.J. Shutts and R. Swinbank, 1986: Alleviation of a systematic westerly bias in general circulation and numerical weather prediction models through an orographic gravity wave drag parameterization. Quart.J.R.Met.Soc., 112, 1001-1039.

Pitcher, E.J., Malone, R.C., Ramanathan, V., Blackmon, M.L., Pain, K. and Bourke, W., 1983: January and July simulations with a spectral general circulation model. J. Atmos. Sci., 40, 580-604.

Shutts, G., 1986: Parameterization of sub-grid scale gravity wave momentum transfer and its influence in forecast/climate models. ECMWF Seminar 1985 p.167-198.

Slingo, A., 1985: Handbook of the Meteorological Office 11-layer atmospheric general circulation models. Met.O 20 DCTN 29. Meteorological Office, Bracknell.

Slingo, A. and D.W. Pearson, 1987: A comparison of the impact of an envelope orography and of a parametrization of gravity-wave drag on simulations with an atmospheric general circulation model. Quart.J.R.Met.Soc., to appear.

Tibaldi, S., 1986: Envelope orography and maintenance of quasi-stationary waves in the ECMWF model. Adv. in Geophys., 29, 339-374.

Von Storch, H., E. Roeckner and U. Cubasch, 1985: Intercomparison of extended-range January simulations with general circulation models: statistical assessment of ensemble properties. Beitr.Phys.Atmosph., 52, 262-286.

Wallace, J.M., and D.S. Gutzler, 1981: Teleconnections in the geopotential height field during the northern hemisphere winter. Mon.Wea.Rev., 109, 784-812.

Wallace, J.M., S. Tibaldi and A.J. Simmons, 1983: Reduction of systematic errors in the ECMWF model through the introduction of an envelope orography. Q.J.Roy.Meteor.Soc., 109, 683-717.